

Copyright
by
David Benjamin Hegermiller
2011

The Thesis committee for David Benjamin Hegermiller
Certifies that this is the approved version of the following thesis:

**A New Method to Incorporate Internal Energy into a
Discrete Velocity Monte Carlo Boltzmann Equation Solver**

APPROVED BY

SUPERVISING COMMITTEE:

Philip Varghese, Supervisor

David Goldstein

**A New Method to Incorporate Internal Energy into a
Discrete Velocity Monte Carlo Boltzmann Equation Solver**

by

David Benjamin Hegermiller, B.S.

THESIS

Presented to the Faculty of the Graduate School of

The University of Texas at Austin

in Partial Fulfillment

of the Requirements

for the Degree of

MASTER OF SCIENCE IN ENGINEERING

THE UNIVERSITY OF TEXAS AT AUSTIN

August 2011

Dedicated to my family who has always supported me in everything I do.

Acknowledgments

I wish to thank my advisors Dr. David Goldstein and Dr. Philip Varghese for their expert advice and guidance. I would also like to thank Paul Bauman for his continued support and willingness to help me solve the many problems and bugs I have encountered through the course of programming this method. I would also like to thank Aaron Morris and Peter Clarke for the many brainstorming sessions we completed together. Lastly, I would like to thank Chris Simmons for giving me the opportunity to work on this project, and PECOS for providing the funding to perform this research.

A New Method to Incorporate Internal Energy into a Discrete Velocity Monte Carlo Boltzmann Equation Solver

David Benjamin Hegermiller, M.S.E.
The University of Texas at Austin, 2011

Supervisor: Philip Varghese

A new method has been developed to incorporate particles with internal structure into the framework of the Variance Reduction method [17] for solving the discrete velocity Boltzmann Equation. Internal structure in the present context refers to physical phenomena like rotation and vibration of molecules consisting of two or more atoms. A gas in equilibrium has all modes of internal energy at the same temperature as the translational temperature. If the gas is in a non-equilibrium state, translational temperature and internal temperatures tend to proceed towards an equilibrium state during equilibration, but they all do so at different relaxation rates. In this thesis, rotational energy of a distribution of molecules is modeled as a single value at a point in a discrete velocity space; this represents the average rotational energy of molecules at that specific velocity. Inelastic collisions are the sole mechanism of translational and rotational energy exchange, and are governed by a modified Landau-Teller equation. The method is tested for heat bath simulations, or homogeneous relaxations, and one dimensional shock problems. Homogeneous relaxations

demonstrate that the rotational and translational temperatures equilibrate to the correct final temperature, which can be predicted by conservation of energy. Moreover, the rates of relaxation agree with the direct simulation Monte Carlo (DSMC) method with internal energy for the same input parameters. Using a fourth order method for convecting mass along with its corresponding internal energy, a one dimensional Mach 1.71 normal shock is simulated. Once the translational and rotational temperatures equilibrate downstream, the temperature, density and velocity, predicted by the Rankine-Hugoniot conditions, are obtained to within an error of 0.5%. The result is compared to a normal shock with the same upstream flow properties generated by the DSMC method. Internal vibrational energy and a method to use Larsen Borgnakke statistical sampling for inelastic collisions is formulated in this text and prepared in the code, but remains to be tested.

Table of Contents

Acknowledgments	v
Abstract	vi
List of Figures	x
Chapter 1. Introduction	1
1.1 Boltzmann Equation Background	1
1.2 Discrete Boltzmann Equation Solvers	3
1.3 Internal Energy in Statistical Methods	5
Chapter 2. Research Background	7
2.1 The Boltzmann Equation	7
2.1.1 The Equation	7
2.1.2 Scaling the Boltzmann Equation	8
2.2 Prior Related Developments in this Research	9
2.2.1 Interpolation Scheme	11
2.2.2 Variance Reduction Method	15
Chapter 3. Theory	19
3.1 Molecular Gas Characteristics	19
3.1.1 Basic Concepts in Statistical Mechanics	19
3.1.2 Translational Energy	20
3.1.3 Internal Energy	23
3.1.3.1 Electronic Excitation	24
3.1.3.2 Rotation	25
3.1.3.3 Vibration	27
3.2 Collision Models	28
3.2.1 Inverse Power Law	30

3.2.2	Hard Sphere Model	32
3.2.3	Variable Hard Sphere Model	33
3.2.4	Variable Soft Sphere Model	35
3.2.5	Maxwell Model	36
3.3	Inelastic Collisions	38
3.3.1	Relaxation Rates	38
3.3.2	Inelastic Collision Model	40
3.3.3	Landau-Teller Equation	43
Chapter 4.	Method	44
4.1	Internal Energy Distribution Function	44
4.1.1	Scaling the Internal Energy Representation	47
4.2	Larsen Borgnakke Method for Inelastic Collisions	49
4.3	New Method for Inelastic Collisions	53
4.3.1	The Method	53
4.3.2	Special Accommodation for Variance Reduction	59
4.3.3	Internal Energy Interpolation Scheme	61
Chapter 5.	Results	65
5.1	Homogeneous Relaxations	65
5.2	1D Normal Shock with Internal Energy	71
5.3	Comparison to DSMC	75
5.4	Convection and Velocity Grid Refinement	79
Chapter 6.	Conclusions	82
6.1	Future Work	83
Bibliography		86
Vita		90

List of Figures

2.1	Sample plot of the cumulative distribution function Ψ	11
2.2	Collision circle showing rotation of the relative velocity vector (g) to points on the grid (g') and points off the grid (g'').	12
2.3	Stencil Showing 3 interior points, 3 exterior points, and an origin . .	13
3.1	The collision parameters b , ϵ and χ	30
3.2	Collision geometry for hard sphere molecules	33
3.3	MATLAB plot showing an example of a VSS re-mapping. The initial relative velocity vector (0,0,4) is rotated by the angles $\chi = \pi/1.3$ and $\epsilon = \pi/3.6$. In the legend, rg_x , rg_y and rg_z represent g'_x , g'_y and g'_z respectively.	36
4.1	A cell in velocity space centered around its respective velocity node. The node has a mass and two internal energy distributions: the rotational and vibrational energy distribution. Each distribution has a set number of energy levels, l , which can be occupied by particles at that velocity node. The population of the energy levels is represented by the height of the spike.	46
4.2	Shows four cases for positive and negative values of $\Delta\hat{\epsilon}$ (the solid blue box) and positive and negative values of the replenishing mass fraction, m_f (the small red box). Above <i>node</i> and <i>node'</i> , the open blue boxes are values of the $\hat{\epsilon}_{\zeta'}$ distribution, and the open red boxes represent the values of $\hat{\phi}_{\zeta'}$. The open blue boxes above the <i>repl</i> represent the value of $\hat{\epsilon}_{\zeta}$. Cases C & D have a negative m_f and Cases B & D have a negative $\Delta\hat{\epsilon}$. The resulting value at point ζ' is seen above the <i>node'</i> label for each case. A is the ideal case where all values are positive. .	64
5.1	Temperature and energy profile for a homogeneous relaxation of rotational and translational energy for initial conditions of $\hat{T}_{rot} = 1$ and $\hat{T}_{tr} = 2$. The method of using the cell translational temperature to define the exchange of energy within the inelastic collision is used here (see Section 4.3.1).	67

5.2	The same case as in Figure 5.1, but the collision energy is used here to define the translational temperature of the collision instead of the cell translational temperature. The scaled final temperature of translation and rotation matches the expected $\hat{T}_{final} = 1.6$ to within 0.5%.	68
5.3	Error between the two options for translational temperature in the inelastic collision. Subscript C represents the cell temperature option used in Figure 5.1, and subscript E represents the collision energy option used in Figure 5.2.	69
5.4	A comparison of the discrete velocity method (DVM) for solving the Boltzmann equation with rotational energy, and the direct simulation Monte Carlo (DSMC) method with rotational energy. $Z_{rot} = 5$ and the x-axis represents the number of equilibrium collisions described by the collision rate, \hat{f} , and the time, t	70
5.5	Rotational and translational temperature profiles for Mach 1.97 normal shock, performed with a physical spacing $a = \Delta x / \lambda_{up} = 1$ and scaled time step $\delta \hat{t} = 0.05$. λ_{up} is the upstream mean free path.	73
5.6	Comparison of Figure 5.5 with a spatially refined and normalized Mach 1.97 normal shock. This normal shock was performed with a physical spacing $a = \Delta x / \lambda_{up} = 0.5$ and scaled time step $\delta \hat{t} = 0.05$. The rotational relaxation collision constant is $Z_{rot} = 5$	74
5.7	Normalized DSMC and DVM temperature profiles for Mach 1.71 monatomic normal shocks. Performed using pseudo-Maxwell molecules for both methods, and for the DVM shock, a uniform velocity space of 13^3 and a scaled velocity grid spacing of $\beta = 0.7$ is used. The physical spacing is $a = 0.5$ and the scaled time step is $\delta \hat{t} = 0.05$. The DSMC shock was obtained using the code DSMC1S.F [5].	76
5.8	Normalized DSMC and DVM temperature profiles for a Mach 1.71 normal shock with rotational energy. The DSMC normal shock is simulated with a relaxation rate corresponding to $Z_{rot} = 5$, whereas for DVM, two cases—a relaxation rate $Z_{rot} = 5$ and 1.25—are shown. . .	77
5.9	Normalized DSMC and DVM temperature profiles for Mach 1.71 normal shock using variable hard sphere and variable soft sphere parameters for nitrogen. The same configuration of physical and velocity space parameters were used as in Figure 5.7	78
5.10	Normalized DSMC and DVM temperature profiles for Mach 1.71 normal shock using VHS for nitrogen. The refined grid is denoted by RG.	80
5.11	Normalized DSMC and DVM temperature profiles for Mach 1.71 normal shock using two different methods for convection.	81

Chapter 1

Introduction

1.1 Boltzmann Equation Background

Fluid dynamics can be broken down into two regimes: the continuum regime, where the Navier-Stokes equations govern the flow, and the rarefied regime, where the Navier-Stokes equations fail. The Boltzmann equation is used to describe non-equilibrium, rarefied gas flows. The rarefied gas regime is characterized by Knudsen numbers greater than or equal to ~ 1 . The Knudsen number is defined as

$$Kn = \frac{\lambda}{L} , \tag{1.1.1}$$

where L is the representative physical length scale and λ is the mean free path. Physically, a Knudsen number approximately greater than 1 means that a molecule travels roughly the problem's characteristic physical length scale between collisions. An example of the physical length scale could be the radius of a body immersed in the fluid.

In the rarefied regime, the Boltzmann equation must be numerically solved to simulate the flow. The direct numerical simulation of the governing Boltzmann equation is computationally expensive. In the most general case, there are three physical

dimensions and three velocity dimensions. Some simple problems require fewer specified dimensions. For example, a one dimensional normal shock can be computed with one spatial dimension and two velocity dimensions. However, as the problem gains complexity, multiple other dimensions can be required to describe internal energy states and species. Therefore, with this multitude of dimensions, the computational cost is very high, and a realistic solver would demand a coarse discretization in velocity space. With coarser grids the accuracy may decrease, and therefore, a trade off between accuracy and computational time exists. The most widely used statistical method that has been shown to approach the Boltzmann equation in certain circumstances is the direct simulation Monte Carlo (DSMC) particle method [5]. This method tracks a finite number of particles and ensemble averages multiple runs to obtain smooth results for the properties at specified points.

For flows which span the continuum and rarefied regimes, a hybrid solver is most efficient. A hybrid solver gains efficiency by using the computationally expensive Boltzmann equation solver or DSMC to solve only the non-equilibrium part of the flow and a less expensive continuum model to solve sections of the flow where it can be employed with reasonable accuracy. For a successful hybrid solver, a low noise interface between the two methods is best. As mentioned previously, DSMC generally achieves smooth flow properties by ensemble averaging many runs. On the other hand, a Boltzmann equation solver can deliver low-noise properties with one run. Therefore if a hybrid solver is required, a direct numerical solver for the Boltzmann equation can prove more efficient than DSMC when employed to achieve a smooth interface between continuum and rarefied regimes.

1.2 Discrete Boltzmann Equation Solvers

The velocities of molecules constituting a gas may be represented by a velocity distribution function. This velocity distribution can be modeled as discrete values which are representative of the velocities of all the particles in the (small) surrounding volume of velocity space. A finer grid of discrete values translates into a more accurate representation of the velocity distribution. The molecular velocities are limited to the specific grid values, but the storage required for every possible velocity point is reduced. The Boltzmann equation then represents the evolution of the mass of particles at these discrete velocity points.

Discrete velocity methods have been used in schemes such as the Hicks-Yen-Nordsieck (HYN) method [18][26] and similarly by Tcheremissine [22]. The HYN method approximates the collision integral by calculating the average collision integral by a Monte Carlo sampling of the integrand. This is only an approximation of the collision integral, and therefore, to enforce conservation of mass, momentum and energy, the HYN method utilizes a correction scheme. This correction scheme may limit the accuracy of the solution. Alternatively, in the Δ - ϵ discrete velocity model developed by Tan and Varghese [21], the collision integral is computed exactly by a Monte Carlo-like selection of velocities for collisions. One shortcoming of this method is that post collision velocities are restricted to lie on the grid, so isotropic scattering is not an option. Furthermore, for high Mach number flows, the velocity space must be very large to accommodate regions of flow with vastly different bulk velocities. An adaptive grid in velocity space would be ideal for this situation.

The Bhatnagar, Gross and Krook (BGK) method [3] solves a linearized colli-

sion integral instead of the full nonlinear collision integral in the Boltzmann equation. The BGK model drives the non-equilibrium distribution towards an equilibrium distribution computed with the local kinetic temperature, velocity and mass. The BGK model does not guarantee the correct rate of relaxation to equilibrium; instead it only guarantees that the flow will relax to an equilibrium distribution.

Morris and Varghese developed the variance reduction method for solving the discrete velocity Boltzmann equation [17]. This method reduces noise in the solution by subtracting the part of the velocity distribution function that has already reached equilibrium and only performing collisions for the remaining non-equilibrium contributions to the collision integral. This reduces computation time significantly, especially in near-equilibrium flows. The interpolation method, developed by Morris, Varghese and Goldstein [15], allows for the remapping of “off grid” post-collision velocities onto the discrete velocity grid while conserving mass, momentum and energy. The interpolation method is not limited to uniform grids and can accommodate velocity points that lie outside the domain of velocity space. Tcheremissine developed a similar interpolation scheme, [20][23][24], to map “off grid” velocities back onto the regularly spaced grid points. His scheme uses the two post-collision velocity points on opposite poles of the collision sphere in conjunction and splits up each mass evenly into two components to be mapped to two nearby velocity nodes. Momentum is automatically conserved by even splitting, and energy is conserved by the symmetric mapping of the two post-collision velocity points. However, this process only works for uniform velocity space grids.

1.3 Internal Energy in Statistical Methods

The relaxation of internal energy with translational energy is an important process in hypersonic flows and other non-equilibrium flows which contain polyatomic molecules. Internal energy relaxation affects key thermodynamic properties of the gas, like the ratio of specific heats. Vibrational modes are generally activated at high temperatures which can be generated by high Mach number shocks. Rotational modes, however, are typically fully excited at room temperature, and the rotational relaxation rate is often on the same order as the translational relaxation rate.

In the framework of the Boltzmann equation, collisions between polyatomic molecules can no longer be considered elastic; an energy exchange must take place between the translational and internal energy modes during collisions. For near equilibrium flows, the general exchange rate of energy was shown by Landau and Teller to follow the Landau-Teller equation [12]. This equation is a finite rate equation that does not specify how internal and kinetic energy are exchanged within inelastic collisions. It simply states that the rate of exchange is proportional to the difference between the translational and internal temperatures. Millikan and White expanded on this equation by developing the relaxation *time* to include a dependence on temperature for many species of gases [13], and Park added a high temperature correction [19]. In the present work, we concentrate on the simple Landau-Teller expressions.

Unlike the discrete velocity methods discussed earlier, DSMC, which tracks specific molecules, uses the inelastic collision method developed by Larsen and Borgnakke [6]. This method statistically selects the post-collision internal energy values by use of an acceptance-rejection scheme. This process in DSMC has been shown in [7] to be

consistent with a Landau-Teller rate of relaxation. Here (in [7]), vibrational levels are described using the simple harmonic oscillator model, which is a good approximation for low vibrational energy levels. However, diatomic molecules behave according to the anharmonic oscillator model for higher vibrational energy levels, and dissociation can occur at or above a certain energy level.

In this thesis, internal energy level distributions are created for rotational and vibrational energy within the framework of a discrete velocity Boltzmann equation solver. However, we will only actually implement rotational energy portion of the model characterized by a single rotational temperature at each point in velocity space, and we will develop an interpolation routine which parallels the velocity interpolation scheme discussed in [15], to remap post-collision internal energy values back on to the grid. The inelastic collision method used is adapted from the Landau-Teller equation, and a homogeneous relaxation example using this method will demonstrate the Landau-Teller relaxation rate. Lastly, a normal shock generated by the discrete velocity Boltzmann equation solver with rotational energy will be compared to a normal shock with rotational energy simulated with the simple DSMC code, DSMC1S.F [5].

Chapter 2

Research Background

2.1 The Boltzmann Equation

So far, we have discussed the Boltzmann equation in name only. This section lays out the Boltzmann equation and its terms. Then the equation is scaled using the characteristic thermal speed η_r and is discretized. At the conclusion of this section, the Boltzmann equation is in a form that can be solved using numerical techniques.

2.1.1 The Equation

The Boltzmann equation describes how the velocity distribution function, φ , evolves over time and space. The general assumptions for the Boltzmann equation as written below are that the gas is infinite and composed of only a single species of particles which interact through elastic binary collisions [11]. This equation can be represented in dimensional form with isotropic scattering while neglecting the effect of body forces [17].

$$\frac{\partial \varphi(\eta_i)}{\partial t} + \eta_i \frac{\partial \varphi(\eta_i)}{\partial x_j} = \int_{\zeta_3} \int_{\zeta_2} \int_{\zeta_1} [\varphi(\eta'_i) \varphi(\zeta'_i) - \varphi(\eta_i) \varphi(\zeta_i)] \hat{g} \sigma_T dV_{\zeta_i} , \quad (2.1.1)$$

where t is time, $\varphi(\eta_i)$ is a single class of atoms or molecules with velocity η_i , $\varphi(\zeta_i)$ is another class of molecules with velocity ζ_i , x_j is the physical location

of spatial cell j , g is the relative speed ($|\zeta_i - \eta_i|$), σ_T is the collision cross section, and dV_{ζ_i} is the differential volume element in velocity space equal to $d\zeta_1 d\zeta_2 d\zeta_3$. For compactness, the triple integral will be written as a single integral over ζ_i , and $\varphi(\eta_i)$ on the left-hand side will be written as just φ from now on.

The left hand side represents the total derivative of the (density weighted) velocity distribution function while the right hand side represents the effects of all molecular collisions on the velocity distribution function. The entire equation is with respect to a single class of molecules with velocity η_i . In this representation, η_i and ζ_i are the pre-collision speeds and η'_i and ζ'_i are the post-collision speeds. We arrive at our definition of the Boltzmann equation from our derivation of the equation based on Vincenti & Kruger [25].

2.1.2 Scaling the Boltzmann Equation

The characteristic thermal speed is the most probable speed for a gas in equilibrium at a reference temperature, T_r , with a molecular mass, m . If we define the characteristic thermal speed as

$$\eta_r = \sqrt{\frac{2k_b T_r}{m}}. \quad (2.1.2)$$

The Boltzmann equation can be scaled by η_r , a reference density n_r , a reference collision cross section σ_r , and a characteristic length L :

$$\hat{t} \equiv t \frac{\eta_r}{L}, \quad \hat{x} \equiv \frac{x}{L}, \quad \hat{\varphi} \equiv \varphi \frac{\eta_r^3}{n_r}, \quad \hat{\sigma}_T \equiv \frac{\sigma}{\sigma_r}, \quad (2.1.3)$$

and

$$\hat{g} \equiv \frac{g}{\eta_r}, \quad \hat{\eta} \equiv \frac{\eta}{\eta_r}, \quad \hat{\zeta} \equiv \frac{\zeta}{\eta_r} . \quad (2.1.4)$$

When the scaling is applied to the Boltzmann equation, it becomes:

$$\frac{n_r}{\eta_r^2 L} \left(\frac{\partial \hat{\varphi}}{\partial \hat{t}} + \hat{\eta}_i \frac{\partial \hat{\varphi}}{\partial \hat{x}_i} \right) = \frac{n_r}{\eta_r^2} n_r \sigma_r \int_{\hat{\zeta}_i} [\hat{\varphi}(\hat{\eta}'_i) \hat{\varphi}(\hat{\zeta}'_i) - \hat{\varphi}(\hat{\eta}_i) \hat{\varphi}(\hat{\zeta}_i)] \hat{g} \hat{\sigma}_T dV_{\hat{\zeta}_i} . \quad (2.1.5)$$

If we define a collision characteristic length as a reference mean free path and the Knudsen number as the reference mean free path divided by the characteristic length we have:

$$L_c = \lambda_r = \frac{1}{n_r \sigma_r} , \quad Kn = \frac{L_c}{L} = \frac{\lambda_r}{L} . \quad (2.1.6)$$

Therefore, the scaled Boltzmann equation is:

$$\frac{\partial \hat{\varphi}}{\partial \hat{t}} + \hat{\eta}_i \frac{\partial \hat{\varphi}}{\partial \hat{x}_i} = \frac{1}{Kn} \int_{\hat{\zeta}_i} [\hat{\varphi}(\hat{\eta}'_i) \hat{\varphi}(\hat{\zeta}'_i) - \hat{\varphi}(\hat{\eta}_i) \hat{\varphi}(\hat{\zeta}_i)] \hat{g} \hat{\sigma}_T dV_{\hat{\zeta}_i} . \quad (2.1.7)$$

2.2 Prior Related Developments in this Research

Previously, this research has focused on developing a direct numerical solver for the Boltzmann equation on a discrete velocity grid. The most direct form of this method centers around colliding each point in velocity space with every other

point in velocity space. This method is referred to as the N^2 method and is very expensive computationally (If N is the number of points in velocity space, then $O(N^2)$ operations are required for each time step). However, we often describe this method as the “Gold Standard” since it produces the most accurate results for the specified velocity grid [17].

Motivated by DSMC methods, the next step in the development of this solver was to employ Monte Carlo selection of velocity grid points for a collision. Points with more mass are chosen more frequently than points with little or no mass. The partial Monte Carlo method was the first developed as a hybrid between the N^2 and a full Monte Carlo technique. All points in the velocity distribution were collided with a random sampling from a cumulative distribution function. This cumulative distribution function is biased towards points which contained more mass. Therefore a random sampling of velocity points from the cumulative distribution led to higher density points being chosen for a collision more often. Full Monte Carlo is the scheme where both collision partners are chosen from the cumulative distribution.

The cumulative distribution function, Ψ , is created by summing up all individual densities of the points in the velocity distribution function, φ . By summing the values in a specific way the three grid indices i, j, k (corresponding to velocity directions x, y, z respectively) can be collapsed onto one index l . This function $\Psi(l)$ is a step function with larger steps representing larger values of mass at a velocity grid point l . An example of $\Psi(l)$ is shown in Figure 2.1 below.

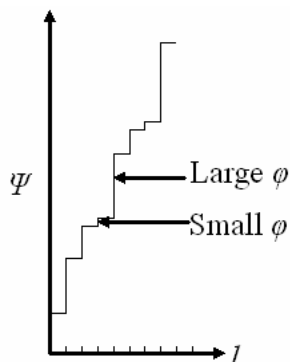


Figure 2.1: Sample plot of the cumulative distribution function Ψ

If i, j, k is summed over all velocity space, and the range of $\Psi(l) = n[0, 1]$ (n is the total number density), then each step represents the probability that that grid point is going to be chosen. This is a more efficient way to implement a Monte Carlo style acceptance rejection routine. Selecting a random number, R_f , from 0 to 1 will then choose the velocity grid point from the cumulative distribution. A set of randomly selected partners can now be chosen that are biased towards areas of the distribution function with larger values. The next part of the development of the code involves two large advances. We will examine each in its own section.

2.2.1 Interpolation Scheme

Collisions are the bread and butter of all Boltzmann equation methods. To understand the interpolation scheme, we must first briefly discuss the dynamics of a collision in the discrete velocity realm. In every collision, two velocity points (η_i and ζ_i) are selected. With these two points we can calculate their relative velocity (g_i) and their center of mass velocity. A certain amount of colliding mass is then depleted

from these points and replenished to two new points that lie on opposite poles of a sphere with a diameter defined by the relative speed. The sphere also contains the original two points which lie on another set of poles. The center of the sphere is defined by the center of velocity of the two points. Figure 2.2 below illustrates this process in two dimensions.

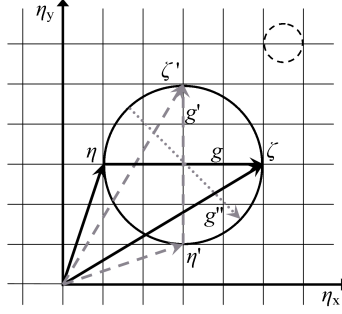


Figure 2.2: Collision circle showing rotation of the relative velocity vector (g) to points on the grid (g') and points off the grid (g'').

There are infinitely many points to choose from that lie off the grid (g''), but only a finite number of points that lie on the grid (g'). Prior to the development of the interpolation scheme by Dr. Philip Varghese (and implemented by Aaron Morris in his thesis [17]) post collision velocities (η') and (ζ') were restricted to lie on the grid. Larger relative velocities allowed for a greater number of “on the grid” pairs; however, for small relative velocities, there may only be one “on the grid” pair (the original collision pair). To permit the post collision velocity pair selection to be more representative of the actual physics of the collision (i.e. to let the rotation of the relative velocity vector be truly random), velocities that lie off the grid (we’ll call them ζ') must be permitted. This requires some sort of interpolation scheme to map that

mass back on the grid while preserving mass, momentum and energy. Therefore, when dealing with a replenishing point that lies off the grid, we have the configuration seen in Figure 2.3. Velocity node points that lie on the grid are represented by a triangle for interior points (points that surround ζ'), a diamond for exterior points and an origin which is always the node closest to ζ' . (Note: the post-collision point must not be near the edge or outside of the allocated velocity space.)

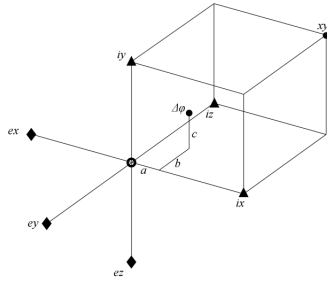


Figure 2.3: Stencil Showing 3 interior points, 3 exterior points, and an origin

The stencil in Figure 2.3 can be made about the post-collision velocity that needs to be interpolated. The function of the interpolation scheme is to map the replenishing mass ($\Delta\varphi$) at the off-grid post collision velocity on to the given velocity grid points. Each point $(o, ix, iy, iz, ex, ey, ez)$ will receive a fraction of $\Delta\varphi$ according to the interpolation matrix seen in [17]. These fractions are seen below in Equation 2.2.1:

$$\begin{aligned}
f_o &= 1 - a^2 - b^2 - c^2 \geq 0, \quad -0.5 \leq a, b, c \leq 0.5, \\
f_{ext} &= -(a + b + c - a^2 - b^2 - c^2)/6 \leq 0, \\
f_{ix} &= (a + f_{ext}), \\
f_{iy} &= (b + f_{ext}), \\
f_{iz} &= (c + f_{ext}).
\end{aligned} \tag{2.2.1}$$

Also, a similar interpolation scheme is produced for post-collision velocities that lie outside the allocated velocity space. Morris describes this method in [17]. The interpolation methods satisfy conservation of mass, momentum and energy; however, one major problem is that negative masses are produced at the exterior points (e_x, e_y, e_z) in order to counteract the increase in kinetic energy associated with splitting the mass over several points.

The mass at a velocity point can be made negative $(-\varphi)$ if a negative mass fraction $(\Delta\varphi < 0)$ that is added to that point is greater than the mass already there. By this means, the solution can develop negative masses at some points, although experience shows they will be small, $O(10^{-4})$, and limited to the wings of the distribution, where there is not much mass in the first place. Previously, this was only a problem for calculating entropy [17], which utilizes the natural logarithm, $\ln(\varphi)$ (we know that the natural logarithm is undefined for $\varphi < 0$). However, as we will see in Section 4, these negative masses will produce negative internal energy according to our definition of the internal energy distribution function. This proves somewhat

problematic for interpolation of internal energy, but we will develop a scheme that preserves total energy (internal + translational) in Section 4.3.3.

2.2.2 Variance Reduction Method

Variance reduction is the latest, most advanced method we have developed for solving the Boltzmann equation numerically. In the variance reduction method, the distribution function is split into two components : $\hat{\varphi} = \hat{\varphi}^{MB} + \hat{\varphi}^d$, where $\hat{\varphi}^{MB}$ is the equilibrium distribution defined by the Maxwellian Boltzmann equilibrium equation below, and $\hat{\varphi}^d$ is the deviation from equilibrium.

$$\hat{\varphi}_{MB} = \frac{\hat{n}}{(\pi\hat{T})^{3/2}} e^{-\hat{\eta}^2/\hat{T}} . \quad (2.2.2)$$

With the split distribution function, the collision integral I_c on the right hand side of the Boltzmann equation seen in Equation 2.1.7 becomes:

$$\begin{aligned} I_c &= \int_{\hat{\zeta}_i} 2[\hat{\varphi}^d(\hat{\zeta}_i')\hat{\varphi}^{MB}(\hat{\eta}_i') - \hat{\varphi}^d(\hat{\zeta}_i)\hat{\varphi}^{MB}(\hat{\eta}_i)]\hat{g}\hat{\sigma}_T d\hat{\zeta}_i \\ &\quad + \int_{\hat{\zeta}_i} [\hat{\varphi}^d(\hat{\zeta}_i')\hat{\varphi}^d(\hat{\eta}_i') - \hat{\varphi}^d(\hat{\zeta}_i)\hat{\varphi}^d(\hat{\eta}_i)]\hat{g}\hat{\sigma}_T d\hat{\zeta}_i \\ &\quad + \int_{\hat{\zeta}_i} [\hat{\varphi}^{MB}(\hat{\zeta}_i')\hat{\varphi}^{MB}(\hat{\eta}_i') - \hat{\varphi}^{MB}(\hat{\zeta}_i)\hat{\varphi}^{MB}(\hat{\eta}_i)]\hat{g}\hat{\sigma}_T d\hat{\zeta}_i \\ &= I_{c1} + I_{c2} + 0 . \end{aligned} \quad (2.2.3)$$

The third collision integral is identically zero because the net change over time of an equilibrium distribution colliding with another equilibrium distribution at the same temperature and density is zero. The derivation of the variance reduction

algorithm is similar to the full Monte Carlo approach in form. However, the equations derived and their implementation are different from the full Monte Carlo version, with the primary benefit being that the algorithm reduces variance in the solution.

The first step of the variance reduction algorithm is to calculate the part of φ that is non-equilibrium, φ^d , and its number density, n_{neq} . The first integral in equation 2.2.3 is solved by drawing a point from the equilibrium distribution function and a point from the non-equilibrium distribution function. The amount depleted from each of the pre-collision points is given by the collision mass, m_{coll} , below:

$$m_{coll} = \frac{sign(\hat{\varphi}^d(\hat{\zeta})) \hat{n} \hat{n}_{neq}}{N_c \beta^3} . \quad (2.2.4)$$

This depletion mass (m_{coll}) is then subtracted from the depletion distribution function, which will contain all the depleted mass for the time step. Performing more collisions has the effect of smoothing the change in the distribution for that time step. N_c , is the number of collisions calculated such that noise is reduced in the system to a specified value (RMS). This equation stems from the requirement that the discretized depletion integral be matched exactly by the statistical model. We calculate N_c using Equation 2.2.5.

$$N_c = nint \left(\frac{\Delta t \hat{n} \hat{n}_{neq}}{RMS^2} \right) \frac{\hat{T}^{(2/3)}}{\beta^3} , \quad (2.2.5)$$

where, $nint()$ represents the value enclosed in the parenthesis rounded to the nearest integer. For the second integral in equation 2.2.3, two points from the non-

equilibrium distribution function are similarly drawn, and the depletion equations are:

$$m_{coll} = \frac{sign(\hat{\varphi}^d(\hat{\eta}))sign(\hat{\varphi}^d(\hat{\zeta}))\hat{n}_{neq}\hat{n}_{neq}}{2N_c\beta^3}, \quad (2.2.6)$$

and

$$N_c = nint \left(\frac{\Delta t \hat{n}_{neq} \hat{n}_{neq}}{2(RMS)^2} \right) \frac{\hat{T}^{(2/3)}}{\beta^3}. \quad (2.2.7)$$

Collisions are then performed, mapped back on to the grid using the interpolation routine given in Section 2.2.1, and the collided mass fractions are added to the replenishing distribution function. (Recall that the colliding mass is subtracted from the depletion function.) At the end of the time step, $\hat{\varphi}$ is updated according to Equation 2.2.8. Note that m_{coll} was subtracted from $\hat{\varphi}_{depl}$ and added to $\hat{\varphi}_{repl}$, so that mass is conserved.

$$\hat{\varphi}' = \hat{\varphi} + \hat{\varphi}_{repl} + \hat{\varphi}_{depl}. \quad (2.2.8)$$

Variance Reduction gains efficiency by not calculating I_{c3} since we know the net result of collisions in I_{c3} is equivalent to zero. This is especially efficient in near-equilibrium flows, where most of the distribution is in equilibrium. Furthermore, the statistical noise around zero is removed from the calculation by the separation of $\hat{\varphi}$ into equilibrium and non-equilibrium parts. Therefore, only the small deviation from equilibrium must be collided and relaxed. However, as we will see in Section

4.3.2, when we include inelastic collisions, we will need to account for the number of collisions in I_{c3} so we can compute the correct internal energy relaxation rate.

Chapter 3

Theory

3.1 Molecular Gas Characteristics

The primary focus of this thesis is to develop a method to incorporate internal energy into the Boltzmann equation. This section will provide the background necessary to understand how internal energy fits in the framework of the particles in our simulation.

3.1.1 Basic Concepts in Statistical Mechanics

Beginning with the Schrödinger wave equation for a particle in a box (see Chapter 4.3 in Vincenti & Kruger [25]), we can solve the equation given the boundary condition that the wave function, ψ , equals zero at the walls. The solution yields the result that the particle energy exists in a discrete form called quantum energy states, which are specified by quantum numbers. Therefore, at any given time, each of the N identical particles in a system will occupy one of the permissible energy states $\epsilon_1, \epsilon_2, \dots, \epsilon_i, \dots$ (where we consider the energy states in a general sense for now).

Typically there exists a difference between Bose-Einstein and Fermi-Dirac statistics (whether or not more than one particle is allowed to be placed in a container). However, in the Boltzmann limit, where temperatures are high enough and

the density is low enough, the likelihood that a state will contain more than one particle is practically nil, even if it is permitted. Therefore, Bose-Einstein and Fermi-Dirac statistics lead to identical results. We lastly define an energy level ϵ_l to contain all the energy states that have identical values of the energy ϵ_i , and the degeneracy of a level g_l as the number of states in a given energy level ϵ_l . We now obtain the number of particles in energy level ϵ_l to be:

$$N_l^* = N \frac{g_l e^{-\epsilon_l/kT}}{Q} , \quad (3.1.1)$$

where Q is the partition function defined as:

$$Q = \sum_l g_l e^{-\epsilon_l/kT} . \quad (3.1.2)$$

The number N_l^* evaluated over all energy levels gives the actual distribution of the particles in a system in equilibrium. This distribution is known as the Boltzmann Distribution. From this we can glean an understanding of how to quantize different energies in a system.

3.1.2 Translational Energy

The previous development of the code has focused on structureless molecules, or molecules that have mass but no internal structure. A simple example of this is any noble gas, whereas an example of a molecule with an internal structure is molecular nitrogen, N_2 . We will examine molecules with an internal structure in the

following section; this section examines translational energy from the standpoint of structureless molecules.

Revisiting partition functions, the translational partition function is given by Equation 3.1.3. For the derivation, see Chapter 4.9 Vincenti & Kruger [25].

$$Q_{tr} = V \left(\frac{2\pi m k T}{h^2} \right)^{3/2} . \quad (3.1.3)$$

Here, V is the volume of the container, m is the mass of the molecule, k is Boltzmann's constant, T is the temperature of the system and h is Planck's constant. If we seek the Boltzmann distribution for translational energy, we use Equation 3.1.1, however we wish to find the number of energy states instead of levels, so we modify the equation to be:

$$N_j^* = N \frac{C_j e^{-\epsilon_j/kT}}{Q} , \quad (3.1.4)$$

where, we know the number C_j of energy states in a group can be found by differentiating Γ , the number of energy states with energy less than ϵ given in Equation 3.1.5.

$$\Gamma = \frac{4\pi V}{3h^3} (2m\epsilon)^{3/2} , \quad (3.1.5)$$

$$C_j = \frac{d\Gamma}{d\epsilon} d\epsilon = 2\pi \frac{V}{h^3} (2m)^{3/2} \epsilon^{1/2} d\epsilon . \quad (3.1.6)$$

We can substitute this in to Equation 3.1.4 and obtain:

$$N_j^* = 2\pi N \frac{\epsilon^{1/2} e^{-\epsilon_j/kT}}{(\pi kT)^{3/2}} d\epsilon . \quad (3.1.7)$$

If we make the substitution $\epsilon = \frac{1}{2}mC^2$, we find the distribution for molecular speed $\chi(C)dC$ seen in Equation 3.1.8 below:

$$\chi(C)dC = 4\pi \left(\frac{m}{2\pi kT} \right)^{3/2} C^2 e^{-mC^2/2kT} dC . \quad (3.1.8)$$

This is the same result for the molecular speed obtained from the Maxwellian velocity distribution using equilibrium kinetic theory. Therefore, the Maxwellian distribution is a special case for translational energy of the more general Boltzmann distribution over translational energy states [25]. Looking ahead, we will see, therefore, that all of our equilibrium distributions are based on the Boltzmann distribution.

Lastly, we can solve for the translational energy E_{tr} of the system and the specific energy ε_{tr} , or the energy per unit mass per molecule:

$$E_{tr} = \frac{3}{2} N k T , \quad (3.1.9)$$

$$\varepsilon_{tr} = \frac{3}{2} R T , \quad (3.1.10)$$

where R is the individual gas constant defined as $R = k/m$. The symbol used for the specific energy and the energy states and levels are very similar. Our usage of ϵ is limited to this section, whereas later in this thesis, we will only be concerned about the specific energy.

3.1.3 Internal Energy

When a molecule has an internal structure, for example a diatomic molecule or monatomic molecule with orbiting electrons, then the other forms of molecular energy cannot be ignored. If we suppose a molecule has a total energy ϵ composed of several independent types of energy $\epsilon = \epsilon' + \epsilon'' + \epsilon''' + \dots$, then keeping with quantum theory, all of these energies must have states. So ϵ' can have values $\epsilon'_1, \epsilon'_2, \dots, \epsilon'_m, \dots$, and likewise ϵ'' can have values $\epsilon''_1, \epsilon''_2, \dots, \epsilon''_n, \dots$; etc. Since an energy state from one type can be taken in conjunction with an energy from another type, we can substitute this into the relation $Q = \sum_i e^{\epsilon_i/kT}$ and obtain the useful property:

$$Q = Q'Q''Q''' \dots \quad (3.1.11)$$

Furthermore, we know the types of energy associated with internal structure. For weakly interacting particles, we can separate ϵ into the translational energy ϵ_{tr} and internal energy ϵ_{int} . ϵ_{int} can be further broken down into a term for electronic excitation energy ϵ_{el} and a term for vibrational and rotational energy. A spinning molecule has a centrifugal field that affects the vibration of the atom, so these two energies are coupled for all but very low temperatures. This coupling between the rotation and vibration of the molecule is very difficult to model, so a simple, but somewhat inaccurate approximation to this problem is separating the rotation and vibration terms. All together, we have the total energy of the molecule and the molecular partition function seen in Equations 3.1.12 and 3.1.13 respectively:

$$\epsilon = \epsilon_{tr} + \epsilon_{rot} + \epsilon_{vib} + \epsilon_{el} , \quad (3.1.12)$$

$$Q = Q_{tr} Q_{rot} Q_{vib} Q_{el} . \quad (3.1.13)$$

Before examining each type of internal energy, we note that the specific internal energy $\varepsilon = E/mN$ behaves according to the following property:

$$\begin{aligned} \varepsilon &= RT^2 \frac{\partial}{\partial T} \ln Q , \\ &= RT^2 \frac{\partial}{\partial T} \ln Q_{tr} + \sum_{int} RT^2 \frac{\partial}{\partial T} \ln Q_{int} , \\ &= \varepsilon_{tr} + \sum_{int} \varepsilon_{int} . \end{aligned} \quad (3.1.14)$$

3.1.3.1 Electronic Excitation

As mentioned before, electronic excitation of a gas can occur for both monatomic and polyatomic gases. For various reasons, the quantum energy levels of an atom or molecule can often be ignored. However, sometimes the levels are degenerate and an electron can pick equally between the states at one energy level. Other times the energy levels can lie in the proximity of the ground (unexcited) level in which case they can be excited easier than levels that lie further away. We begin with Equation 3.1.2. If we expand this out and replace $\epsilon_l/k = \Theta_l$, the characteristic temperature for electronic excitation, we have:

$$Q_{el} = Q = \sum_l g_l e^{-\epsilon_l/kT} = g_0 e^{-\Theta_0/T} + g_1 e^{-\Theta_1/T} + g_2 e^{-\Theta_2/T} + \dots \quad (3.1.15)$$

We can obtain values for Θ_l from the tabulated data in Moore [14]. The typical convention is to make ϵ_0 equal to zero and base the other energy levels off that “ground” level [25]. Since the values for Θ are typically large, only the first one or two energy levels are significantly populated. Therefore, it is a fair approximation that for relatively low temperatures, the partition function can reasonably be defined with one excitation level as $Q_{el} = g_0 + g_1 e^{-\Theta_1/T}$. Using this definition, the specific internal energy for electronic excitation ε_{el} is given below:

$$\varepsilon_{el} = R\Theta_1 \frac{(g_1/g_0)e^{-\Theta_1/T}}{1 + (g_1/g_0)e^{-\Theta_1/T}}. \quad (3.1.16)$$

3.1.3.2 Rotation

Rotation and vibration enter the picture when the molecules are polyatomic, no longer monatomic. For this point in the development of this research, assuming the gas consists of only diatomic molecules will suffice. This turns out to be a good assumption, since the primary gases in the atmosphere are diatomic. This section will deal with rotation and the next will deal with vibration.

We characterize the diatomic molecule as a dumbbell with a moment of inertia I . Solving the Schrödinger equation, it is found that the degenerate energy levels are given as

$$\epsilon_l = \frac{h^2}{8\pi^2 I} l(l+1) , \quad \text{where } l = 0, 1, 2, \dots \quad (3.1.17)$$

Due to different axes of rotation, the degeneracy is then by $g_l = 2l + 1$, and the rotational partition function is

$$\begin{aligned} Q_{rot} &= \sum_{l=0}^{\infty} (2l+1) \exp \left[\frac{-l(l+1)h^2}{8\pi^2 I k T} \right] , \\ &= 1 + 3e^{-2\Theta_r/T} + 5e^{-6\Theta_r/T} + \dots \end{aligned} \quad (3.1.18)$$

Θ_r is the characteristic temperature of rotation defined as

$$\Theta_r \equiv \frac{h^2}{8\pi^2 I k} , \quad (3.1.19)$$

which has units of Kelvin. Numerical data for Θ_r can be found in Herzberg [9]. Typical values of Θ_r are small; on the order of 10^0 to 10^1 Kelvin (i.e. for nitrogen (N_2), $\Theta_r = 2.9K$), so that even at room temperature, many rotational energy levels are excited. Therefore an accurate approximation for the partition function is $Q_{rot} = T/\sigma\Theta_r$. Here the symmetry factor σ has been introduced to account for the type of diatomic molecule we are dealing with: $\sigma = 1$ for heteronuclear molecules and $\sigma = 2$ for homonuclear molecules. Solving for the specific energy of rotation ϵ_{rot} , we obtain:

$$\epsilon_{rot} = RT . \quad (3.1.20)$$

If we recall the Boltzmann distribution in Equation 3.1.1, we can apply that for each of the rotational energy levels and obtain the number density at each energy level. This would be useful if we desired to have a distribution curve for the rotational energy.

3.1.3.3 Vibration

We will consider vibration also in the framework of a diatomic molecule. For this, we can reasonably assume that the molecule is a harmonic oscillator with frequency ν . Therefore, we have energy levels defined as

$$\epsilon_i = ih\nu, \quad \text{where } i = 0, 1, 2, \dots \quad (3.1.21)$$

And our vibrational partition function follows as

$$Q_{vib} = \sum_{i=0}^{\infty} e^{-ih\nu/kT}. \quad (3.1.22)$$

Using the definition of the characteristic temperature of vibration $\Theta_\nu \equiv h\nu/k$ and the geometric series for $x = e^{-h\nu/kT}$ we obtain:

$$Q_{vib} = \frac{1}{1 - e^{-\Theta_\nu/T}}. \quad (3.1.23)$$

Solving for the the specific vibrational energy ε_{vib} we have the equation:

$$\varepsilon_{vib} = \frac{R\Theta_\nu}{e^{\Theta_\nu/T} - 1}. \quad (3.1.24)$$

Recall that this specific vibrational energy was derived with the simple harmonic oscillator assumption. This is not always the case, and for excitation to higher vibrational levels, the molecule experiences anharmonic effects. These can be incorporated by computing the specific energy level transitions, as it has been shown in Adamovich *et al.* [1]. When the vibrational energy levels become high enough, they approach a dissociation energy, D . Above a certain energy level, the molecule will dissociate, producing atoms of the molecule's components. Currently the formulation of the Boltzmann equation we have developed cannot handle dissociation, chemistry or multiple species, so we choose to assume the simple harmonic oscillator approximation.

We may desire to track the population of the different levels of the vibrational energy, as vibrational energy typically plays a large role in the relaxation of high temperature non-equilibrium problems, like a shock wave. For this we can utilize the Boltzmann distribution in Equation 3.1.1 to find the number density of the vibrational states during a relaxation. However, the Boltzmann distribution assumes the gas is in equilibrium; therefore, if non-equilibrium effects are desired within the vibrational energy distribution, then a more detailed model of non-equilibrium kinetics will be necessary.

3.2 Collision Models

In order to understand how molecules exchange energy, we must examine the dynamics of collisions. Within elastic collisions, kinetic (translational) energy is conserved, whereas inelastic collisions conserve only the total energy of the collision. The

total energy is the sum of translational, vibrational, rotational and electronic excitation energy ($\varepsilon_{tot} = \varepsilon_{tr} + \varepsilon_{vib} + \varepsilon_{rot} + \varepsilon_{el}$). We will examine inelastic collisions in Section 3.3. This section examines elastic collisions and the different models we can utilize to best represent the collision.

There are several molecular models used to describe the intermolecular interactions. Each of the models defines a the total collision cross-section, σ_T , which is required for the Boltzmann Equation (see Equation 2.1.1) To find σ_T , first we define the differential collision cross-section as:

$$\sigma d\Omega = b db d\epsilon , \quad (3.2.1)$$

where b is the miss distance (impact parameter) and ϵ is the angle between a reference plane and the collision plane. The scattering angle χ is the angle post collision relative velocity vector, g' makes with the relative velocity vector g . These parameters can be seen in Figure 3.1 [5].

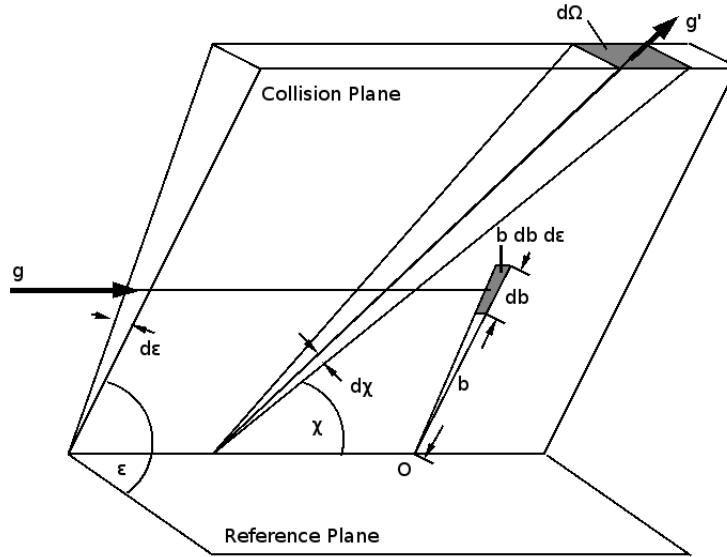


Figure 3.1: The collision parameters b , ϵ and χ

Lastly we can find the total collision cross-section by integrating the differential collision cross-section:

$$\sigma_T = \int_0^{4\pi} \sigma d\Omega = 2\pi \int_0^\pi \sigma \sin\chi d\chi. \quad (3.2.2)$$

3.2.1 Inverse Power Law

We will start this discussion with the generic inverse power law for the inter-molecular force F :

$$F = \frac{\kappa}{r^\eta}. \quad (3.2.3)$$

Here κ is the inverse power law constant, r is the radius from the center of the collision and η is the inverse power law exponent. The inverse power law is often, although not exclusively called the point center of repulsion model, and we notice that as the radius decreases, the repulsive force increases. We can also express this force as a potential energy ϕ :

$$\phi = \frac{\kappa}{(\eta - 1)r^{\eta-1}} . \quad (3.2.4)$$

It is useful to write the ratio of the potential energy to the asymptotic kinetic energy to derive a second dimensionless impact parameter, W_0 [5]. This is given in [5] as:

$$\frac{\phi}{\frac{1}{2}m_r g^2} = \frac{2\kappa m_r g^2}{(\eta - 1)r^{\eta-1}} = \frac{2}{\eta - 1} \left(\frac{W}{W_0} \right)^{\eta-1} , \quad (3.2.5)$$

with W and W_0 given by:

$$W = \frac{b}{r} (m_r g^2)^{2/(\eta-1)} \quad W_0 = b \left(\frac{m_r g^2}{\kappa} \right)^{1/(\eta-1)} . \quad (3.2.6)$$

We can then write the scattering angle, χ , as:

$$\chi = \pi - 2 \int_0^{W_1} [1 - W^2 - [2/(\eta - 1)](W/W_0)^{\eta-1}]^{-1/2} dW , \quad (3.2.7)$$

and W_1 is given by the positive root of

$$1 - W^2 - [2/(\eta - 1)](W/W_0)^{\eta-1} = 0 . \quad (3.2.8)$$

We see that χ is only a function of W_0 and therefore we can substitute into Equation 3.2.1 to obtain the collision cross-section for the inverse power law model in Equation 3.2.9:

$$\sigma d\Omega = W_0 \left(\frac{\kappa}{m_r g^2} \right)^{2/(\eta-1)} dW_0 d\epsilon . \quad (3.2.9)$$

For finite values of η the force field extends to infinity and the integral in Equation 3.2.2 for the total collision cross-section diverges. This means that the total collision cross-section is infinite; however, for practical models there needs to be some cutoff specified for either the distance of closest approach, b , or the scattering angle, χ [5]. These adjustments to the model are the focus of later models which will be described in the following sections.

3.2.2 Hard Sphere Model

The hard sphere model is simply explained by imagining two billiard balls colliding. They exert no force on each other until the instant they are in contact and then immediately after contact, they once again exert no force on each other. Mathematically, the hard sphere model is given by the inverse power law when $\eta = \infty$. Therefore the force is then only effective when the molecules just touch at the distance of closest approach, where $r = 1/2(d_1 + d_2) = d_{12}$. By the geometry in Figure 3.2 the miss distance, b , at the radius of closest approach, is given below [5].

$$b = d_{12} \cos(\chi/2) = d_{12} \sin(\theta_A) . \quad (3.2.10)$$

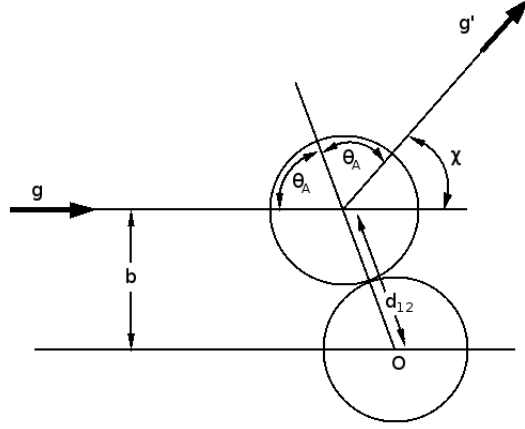


Figure 3.2: Collision geometry for hard sphere molecules

The apse angle, θ_A is defined by $\chi + 2\theta_A = \pi$ when the radius is d_{12} . Plugging into Equation 3.2.2, the total collision cross-section is πd_{12}^2 :

$$\sigma_T = \int_0^{4\pi} \frac{1}{4} d_{12}^2 d\Omega = \pi d_{12}^2 . \quad (3.2.11)$$

The advantage to the Hard Sphere model is that the collision cross-section is finite and the scattering angle is isotropic, meaning that all directions are equally probable.

3.2.3 Variable Hard Sphere Model

The Variable Hard Sphere (VHS) model shares the important characteristics of the Hard Sphere model, i.e. isotropic scattering and a finite cross-section. However, the cross-section decreases as the relative speed, g , and therefore, kinetic energy, E_{tr} ,

increases. To grasp this, realize faster moving particles have less time for their forces to interact. The VHS model addresses this issue by making the hard sphere diameter a function of the relative speed according to the following equation:

$$d = d_{ref} \left(\frac{g_{ref}}{g} \right)^\omega . \quad (3.2.12)$$

The subscript $()_{ref}$ denotes reference values and ω is the coefficient of viscosity, which depends on the type of gas. We can now obtain the total collision cross-section for variable hard sphere particles as

$$\sigma_T = \sigma_{ref} \left(\frac{g}{g_{ref}} \right)^{-\omega} . \quad (3.2.13)$$

Since this follows a power law format with a real gas temperature exponent of the coefficient of viscosity, Bird was able to define a mean free path (λ) and a Knudsen number with this model [4]. Recall that both the Knudsen number and λ are used in the Boltzmann equation (see Section 2.1.2).

The viscosity index, ω , is a constant for each type of gas. Real gas values for ω range from 0.5 to ~ 1 (ammonia has a viscosity index of 1.1), and can be found in Appendix A, Table A1 of Bird [5]. If ω is set equal to 1.0, the VHS model reduces to Maxwell molecules, and if $\omega = 0.5$ we obtain pseudo-Maxwell molecules (Maxwell molecules will be discussed in Section 3.2.5). Lastly, if ω is set equal to 0.0, the model reduces to the hard sphere model.

3.2.4 Variable Soft Sphere Model

The Variable Soft Sphere (VSS) model [10], uses the same adjustment to the diameter as the VHS model; therefore, the total collision cross-section σ_T is πd^2 . However, VSS corrects for the isotropic scattering deficiency; the scattering angle is now given by:

$$\chi = 2\cos^{-1} \left[\left(\frac{b}{d} \right)^{1/\alpha} \right] . \quad (3.2.14)$$

Since the scattering is no longer isotropic for VSS, we have to use a new re-mapping scheme for the post collision relative velocity vector. The ‘re-mapping’ scheme orients the post-collision relative velocity vector, $g' = (g'_x, g'_y, g'_z)$ with respect to the original relative velocity vector, $g = (g_x, g_y, g_z)$. The equations to find the new position of g' are given in Koura & Matsumoto [10] as:

$$\begin{aligned} g'_x &= \frac{1}{2} \left[g_x \cos(\chi) + \frac{\sin(\chi) [g g_y \cos(\epsilon) - g_z g_x \sin(\epsilon)]}{(g_x^2 + g_y^2)^{1/2}} \right] , \\ g'_y &= \frac{1}{2} \left[g_y \cos(\chi) - \frac{\sin(\chi) [g g_x \cos(\epsilon) + g_z g_y \sin(\epsilon)]}{(g_x^2 + g_y^2)^{1/2}} \right] , \\ g'_z &= \frac{1}{2} [g_z \cos(\chi) + \sin(\epsilon) \sin(\chi) (g_x^2 + g_y^2)^{1/2}] . \end{aligned} \quad (3.2.15)$$

Notice in Equation 3.2.15, the parameter $(g_x^2 + g_y^2)^{1/2}$ in the denominator of the g'_x and g'_y equations. For any random selection, i , of a colliding pair on a structured velocity grid, the relative velocity g_i may be aligned with the z direction so that $g_x = g_y = 0$. Therefore, the denominator is identically zero and a numerical

issue can arise. However, it can be shown that the limit exists as g_x and g_y go to zero, so we use the limit when we would be forced to divide by zero. Figure 3.2.4 on the next page shows that the limit exists as g_x and g_y go to zero.

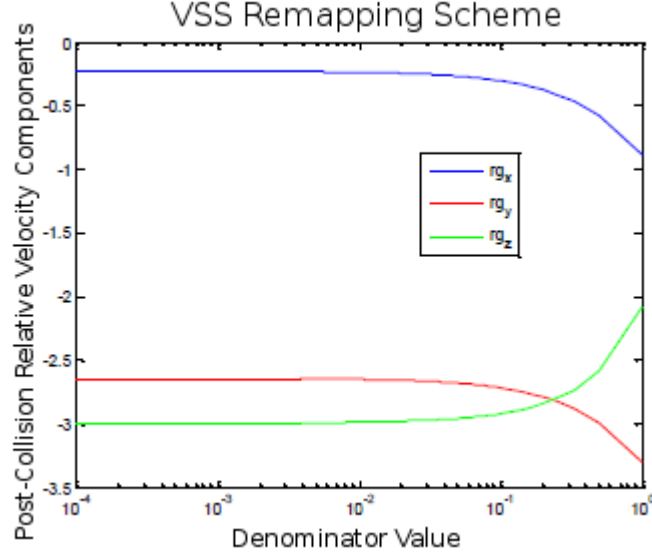


Figure 3.3: MATLAB plot showing an example of a VSS re-mapping. The initial relative velocity vector (0,0,4) is rotated by the angles $\chi = \pi/1.3$ and $\epsilon = \pi/3.6$. In the legend, rg_x , rg_y and rg_z represent g'_x , g'_y and g'_z respectively.

Typical values of α range from 1 to 2 (i.e. nitrogen has $\alpha_{N_2} = 1.36$, and methane has $\alpha_{CH_4} = 1.60$). Lastly, if we set α equal to 1.0, we reduce the VSS model to the Maxwell model which is discussed below.

3.2.5 Maxwell Model

The Maxwell model is the case for the inverse power law where $\eta = 5$. Plugging in, we arrive at the result for the differential collision cross-section [5] given by:

$$\sigma d\Omega = \frac{W_0}{g} \left(\frac{\kappa}{m_r} \right)^{1/2} dW_0 d\epsilon . \quad (3.2.16)$$

The collision probability for a pair of molecules is proportional to the product of the collision cross-section and the relative velocity. If we multiply Equation 3.2.16 by the relative velocity, g , we see that the collision probability is independent of the relative velocity for Maxwell molecules.

The Maxwell model is also useful in solving the Boltzmann equation, since the only known analytical solution for the Boltzmann equation far from equilibrium is for a Bobylev Krook Wu (BKW) homogeneous relaxation using Maxwell, or pseudo-Maxwell molecules [11]. Therefore, using Maxwell molecules in a simulation of the BKW relaxation by our discrete velocity direct simulation Boltzmann solver will yield a comparison to an analytical solution.

Lastly, the Maxwell model can be considered the limiting case for 'soft' molecular models. Similarly, the hard sphere model is the limiting case for 'hard' molecular models. The full range of previously discussed molecular models are available for use in the DVM code by adjusting the VHS and VSS parameters as discussed in Sections 3.2.3 and 3.2.4. The previous research has focused on using pseudo-Maxwell molecules for the discrete velocity Boltzmann equation solver; however, for the rest of the paper, we prefer to keep the collision model general. A note will be made wherever a specific collision model is relevant.

3.3 Inelastic Collisions

We continue the discussion of collision dynamics by introducing internal energy. Collisions are now inelastic; translational energy can be exchanged with rotational, vibrational and electronic excitation energy. In physical collisions all forms of energy may be exchanged with one another. Different energy levels within one energy mode can exchange energy as well. However, we will begin this discussion by assuming that internal energy only exchanges with translational energy and only one type of energy transfer happens per collision. For example, an inelastic collision will exchange either translational and rotational, translational and vibrational or translational and electronic excitation energy. A certain fraction of the collisions will remain elastic. Mass, momentum and energy are still conserved within collisions, but now the energy may be exchanged between translational and internal energy modes too.

3.3.1 Relaxation Rates

We assume here that the exchange between translational energy, E_{tr} and internal energy, E_{int} , can be modeled approximately by the difference between the translational and internal temperatures and a relaxation time, τ_{int} . The relaxation time is unique for each type of gas and different for the various internal energy modes. It is typically a function of temperature and density. When the temperature is changing, numerical methods must be used to compute the relaxation time, but for a simple heat bath where the gas is maintained at a specific temperature, τ_{int} is reasonably assumed to be a constant. We can make the assumption that the relaxation time

is constant, even in non-equilibrium problems. However, just how accurate this assumption is depends on the type of internal energy being considered [25].

The primary focus in the development of relaxation time theory has been in vibrational relaxation. Rotational relaxation and vibrational relaxation rates are both dependent on the translational temperature. However, the rotational relaxation time typically only changes by a small amount (1-10 collision times) over a range of temperatures, while the vibrational relaxation time can go from 10,000 collision times (τ_{coll}) at low translational temperature, to 1 τ_{coll} at very high translational temperatures. Therefore, although approximating the rotational relaxation time by a constant is not an accurate assumption, it is a better than approximating the vibrational relaxation time by a constant. A more exact equation for the vibrational relaxation time is required since the model will lose accuracy as large temperature changes are introduced.

We will continue this discussion only for the vibrational relaxation time τ_v . When the pressure and temperature are not constant in a non-equilibrium high temperature problem, the relaxation time now becomes a local relaxation time and takes the form $\tau = \tau(p, T)$. Landau and Teller [12] obtained an approximate expression for the local relaxation time of the form:

$$\tau = \frac{K_1 T^{5/6} e^{(K_2/T)^{1/3}}}{p(1 - e^{-\Theta_v/T})} , \quad (3.3.1)$$

where K_1 and K_2 are positive constants depending on the type molecules involved. These parameters can be estimated by experimentally measured relaxation

times. Furthermore, using this relaxation time, we can calculate the approximate number of collisions required to produce vibrational equilibrium. We know from Vincenti & Kruger [25], that a single molecule at $p = 1 \text{ atm}$ and $T_o = 273 \text{ K}$ experiences approximately 10^{10} collisions per second. If we assume pressure is constant and we are using hard sphere molecules, the frequency of collisions, ϱ , can be put in terms of the temperature of the distribution. Therefore, we have:

$$\varrho(T) = \sqrt{\frac{T_o}{T}} \varrho(T_o) , \quad (3.3.2)$$

and the number of collisions to reach equilibrium is $N_{coll_{eq}} = \tau_v \varrho(T)$. If we take oxygen, O_2 , at $p = 1 \text{ atm}$ and $T_o = 273 \text{ K}$, we expect approximately 18000 collisions to achieve equilibrium conditions in vibration. (This is based on the data given in [25].) This number is large compared to the number for rotational/translational energy exchange, which is on the order of 10 collisions. Therefore, it is much more important to accurately represent the vibrational relaxation time, than the rotational relaxation time.

3.3.2 Inelastic Collision Model

Inelastic collisions can be viewed as occurring in either of two ways; either a certain fraction (say $\frac{1}{Z}$) of the total collisions are inelastic, or all collisions are inelastic except the energy transfer is now $\frac{1}{Z}$ times what it was before, but happens on every collision. While the former argument may be computationally less expensive, the latter argument may yield more continuous or stable results. The fraction, $\frac{1}{Z}$, discussed here takes the form of a number which is derived from experimental tests of

translational, rotational and vibrational relaxation times (see the pertinent discussion in Section 3.3.1). This number Z is either Z_{rot} (rotational) or Z_{vib} (vibrational). A typical number for Nitrogen, N_2 , would be $Z_{rot} = 5$. For now, we will assume that Z is a constant, independent of temperature.

The model developed here for inelastic collisions contains two different types of collisions: ones with translational and rotational energy transfer (T-R collisions), and ones with translational and vibrational energy transfer (T-V collisions). For simplicity, there are no collisions where we consider the exchange between rotational and vibrational energy directly or an exchange between all three types. Therefore, if we think in terms of an inelastic collision happening every Z collisions, we recognize that a fraction ($\frac{1}{Z_{tr}}$) of collisions will be purely elastic. We also notice that the three different Z values must obey the following property:

$$\frac{1}{Z_{tr}} + \frac{1}{Z_{rot}} + \frac{1}{Z_{vib}} = 1 . \quad (3.3.3)$$

Therefore, for any given time step, three different types of collisions are going to be occurring: elastic collisions where E_{tr} is unchanged (T-T), collisions where E_{tr} is exchanged with E_{rot} (T-R) and collisions where E_{tr} is exchanged with E_{vib} (T-V).

We now calculate the total number of collisions per time step, N_{ctot} , for the Variance Reduction Method by summing all the allotted collisions for the three collision integrals: $\int_C = \int_{MB-MB} + \int_{MB-\delta} + \int_{\delta-\delta}$ (see Section 2.2.2 for a discussion of the split collision integral). The total number of collisions is:

$$N_{c_{tot}} = n_{int} \left(\frac{\delta \hat{t}}{RMS^2} \left[\frac{\hat{n}^2}{2} + \hat{n} \hat{n}_\delta + \frac{\hat{n}_\delta^2}{2} \right] \right) \frac{\hat{T}^{(2/3)}}{\beta^3} , \quad (3.3.4)$$

where the derivation for Equation 3.3.4 is derived from the equations in [17]. Note that the collisions for $\int_{MB-\delta}$ and $\int_{\delta-\delta}$ will be performed using the method outlined in Sections 4.2 and 4.3, while collisions in \int_{MB-MB} are not calculated so the energy exchange must be dealt with differently. This is discussed in greater detail in Section 4.3.2. Since we calculate the total number of collisions in Equation 3.3.4, we can obtain the number of collisions performed for each type of exchange: $N_{c_{T-T}}$ for T-T collisions, $N_{c_{T-R}}$ for T-R collisions and $N_{c_{T-V}}$ for T-V collisions. Also note that we will only need to specify two Z values, so we choose $Z_{tr} = Z_{tr}(Z_{rot}, Z_{vib})$, and solve for it using Equation 3.3.3. Therefore, we have:

$$N_{c_{T-T}} = \left(1 - \frac{1}{Z_{rot}} - \frac{1}{Z_{vib}} \right) N_{c_{tot}} , \quad (3.3.5)$$

$$N_{c_{T-R}} = \frac{1}{Z_{rot}} N_{c_{tot}} , \quad (3.3.6)$$

$$N_{c_{T-V}} = \frac{1}{Z_{vib}} N_{c_{tot}} . \quad (3.3.7)$$

Variance Reduction divides up $N_{c_{tot}}$ so that different parts of the collision integral are calculated separately. We can obtain $N_{c_{T-T}}$, $N_{c_{T-R}}$ and $N_{c_{T-V}}$ for each piece of the collision integral using the equations above since we know the number of collisions performed for each integral (see Section 2.2.2).

3.3.3 Landau-Teller Equation

A homogeneous isotropic perturbed gas dynamic system will approach equilibrium over time. Knowing the relaxation time, we can model the exchange rate between translational and internal energy. The most simple approach is to use the Landau-Teller equation [12], to describe this exchange.

$$\frac{dE_{int}}{dt} = \frac{E_{int}(T_{tr}) - E_{int}(T_{int})}{\tau_{int}} = \frac{E_{int}(T_{tr}) - E_{int}(T_{rot})}{Z_{int}\tau_{coll}}, \quad (3.3.8)$$

where $\tau_{int} = Z_{int}\tau_{coll}$ is the relaxation time for that particular form of internal energy, and $E_{int}(T_{tr})$ is the internal energy evaluated at the translational temperature. More simply, this energy exchange can be written to describe the temperature equilibration:

$$\frac{dT_{int}}{dt} = \frac{T_{tr} - T_{int}}{Z_{int}\tau_{coll}}. \quad (3.3.9)$$

If $Z_{int} \geq 1$, we see that the internal energy equilibration with translational energy is always slower than the translational energy equilibration. Therefore, even after the velocity distribution has approached a quasi-equilibrium, we will see the effects of internal energy on the translational temperature of the gas distribution as energy is exchanged with internal energy levels at a slower rate. The internal energy distribution will continue to change until the the internal temperature is in equilibrium with the translational temperature, which is relaxing as well.

Chapter 4

Method

This section will outline two methods for performing inelastic collisions in the framework of the Boltzmann equation. The first is the Larsen Borgnakke method [6] used commonly in DSMC and adapted here to be used in our discrete velocity direct simulation Boltzmann solver. The second is what we call the “New Method” which was developed by Dr. Varghese and myself as an adaptation of the Landau-Teller equation to be more representative of known gas dynamics and to be amenable to the variance reduction approach. Both methods center around describing what happens within an inelastic collision. We will discuss both approaches, with a greater focus on the New Method in Section 4.3. However, first we must describe how we represent internal energy in the framework of the discrete velocity Boltzmann equation.

4.1 Internal Energy Distribution Function

We know from our discussion in Section 3.1.1 that molecules can occupy a number of energy states, with the equilibrium population distribution of those states governed by the Boltzmann distribution in Equation 3.1.1. Therefore within a small volume of velocity space there is a given number density of particles. The density normalized velocity distribution, φ , stores the percentage of molecules with a certain

velocity η_i , at spatial node x_i and time t .

$$\varphi = n f(x_i, \eta_i, t) , \quad (4.1.1)$$

where $f(x_i, \eta_i, t)$ is the probability that that a molecule has a velocity within dV_η of η_i . We normalize f by the following equation:

$$\int_{V_\eta} f dV_\eta = 1 . \quad (4.1.2)$$

Knowing the number density of particles at a specified velocity, we can sort those particles into a number of internal energy levels. If the gas is in equilibrium, the internal energy distribution of the particles will follow the Boltzmann distribution for the temperature of the gas. However, in non-equilibrium flows, the number density of any of the levels will not necessarily be the Boltzmann number density for that level. Therefore, it is desired to have a number, l_r , of rotational energy levels and l_v vibrational energy levels to describe non-equilibrium situations.

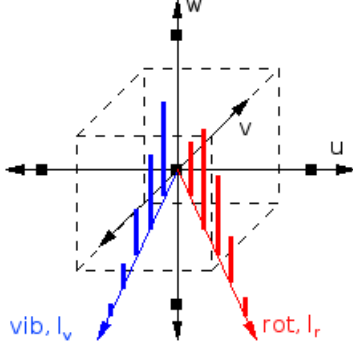


Figure 4.1: A cell in velocity space centered around its respective velocity node. The node has a mass and two internal energy distributions: the rotational and vibrational energy distribution. Each distribution has a set number of energy levels, l , which can be occupied by particles at that velocity node. The population of the energy levels is represented by the height of the spike.

In order to achieve generality, we will represent the internal energy distributions in this section as having l energy levels. Now we define φ_ε to include the internal energy per unit mass distributions: $\varepsilon_{rot}(l_r, x_i, \eta_i, t)$ for rotational energy and $\varepsilon_{vib}(l_v, x_i, \eta_i, t)$ for vibrational energy:

$$\varphi_{\varepsilon_{rot}} = nf(x_i, \eta_i, t)\varepsilon_{rot}(l_r, x_i, \eta_i, t) , \quad (4.1.3)$$

$$\varphi_{\varepsilon_{vib}} = nf(x_i, \eta_i, t)\varepsilon_{vib}(l_v, x_i, \eta_i, t) . \quad (4.1.4)$$

That is, $\varphi_{\varepsilon_{rot}}$ and $\varphi_{\varepsilon_{vib}}$ are the total internal energy distributions, where if one point in velocity space is selected, $\varphi_{\varepsilon_{rot}}(l_r)$ and $\varphi_{\varepsilon_{vib}}(l_v)$ would represent the total number density of all particles occupying internal energy level l_r or l_v at that velocity. Since this is the first iteration of an internal energy method, we choose to describe

all the particles at a single point in velocity space as occupying a single internal energy level that has the average internal energy of all the particles at that velocity. Therefore, our current case will have $l_r = l_v = 1$, and since $\varphi = n f(x_i, \eta_i, t)$ stores the number density of particles at that velocity point, the average internal energy value is stored in the $\varepsilon(1, x_i, \eta_i, t)$ distribution.

4.1.1 Scaling the Internal Energy Representation

We will begin by analyzing rotational energy and then extend the concept to vibrational energy. Since for each internal energy mode, we are dealing with the average internal energy of molecules at a specific discrete velocity, we represent rotational energy at that discrete velocity as $E_{rot} = kT$ or the rotational energy per molecule. Here we assume the gas is in equilibrium, so T is used. We can begin scaling the equation using, $T = T_{ref} \hat{T}$.

$$E_{rot} = k T_{ref} \hat{T} . \quad (4.1.5)$$

If we divide both sides by the mass of the molecule and multiply the right side of the equation by $\frac{2}{2}$, we obtain the internal energy per molecule per unit mass. This is the specific rotational energy we found in Section 3.1.3.2.

$$\varepsilon_{rot} = \frac{E_{rot}}{m} = \frac{2k T_{ref}}{m} \frac{\hat{T}}{2} . \quad (4.1.6)$$

Recognize that the quantity $\eta_r^2 = \frac{2k T_{ref}}{m}$ is the reference velocity squared. We can divide both sides of the equation by η_r^2 to obtain the scaled rotational energy:

$$\hat{\varepsilon}_{rot} = \frac{\varepsilon_{rot}}{\eta_r^2} = \frac{\hat{T}}{2} . \quad (4.1.7)$$

We can use the same operations on the vibrational energy. Beginning with our definition of the equilibrium vibrational energy per molecule assuming a harmonic oscillator, we have:

$$E_{vib} = \frac{k\Theta_v}{e^{\Theta_v/T} - 1} . \quad (4.1.8)$$

Scaling temperature again with $T = T_{ref}\hat{T}$ and multiplying the numerator by $\frac{T_{ref}}{T_{ref}}$, we obtain:

$$E_{vib} = \frac{k T_{ref} \frac{\Theta_v}{T_{ref}}}{\exp \left[\frac{\Theta_v}{T_{ref} \hat{T}} \right] - 1} . \quad (4.1.9)$$

We define the parameter $\hat{\Theta}_v = \frac{\Theta_v}{T_{ref}}$ as the scaled characteristic temperature of vibration. If we divide both sides of the equation by m and multiply the right side by the factor $\frac{2}{2}$ we obtain the vibrational energy per molecule per unit mass, or the specific vibrational energy we saw in Section 3.1.3.3:

$$\varepsilon_{vib} = \frac{E_{vib}}{m} = \frac{\frac{2k T_{ref}}{m} \hat{\Theta}_v}{2 \exp \left[\frac{\hat{\Theta}_v}{\hat{T}} \right] - 1} . \quad (4.1.10)$$

Notice the factor $\eta_r = \left(\frac{2k T_{ref}}{m} \right)^{1/2}$ in the numerator again, so dividing by η_r^2 we obtain the scaled specific vibrational energy:

$$\hat{\varepsilon}_{vib} = \frac{\varepsilon_{vib}}{\eta_r^2} = \frac{\hat{\Theta}_v}{2 \left[\exp(\hat{\Theta}_v/\hat{T}) - 1 \right]} . \quad (4.1.11)$$

The definitions of scaled specific internal energy, $\hat{\varepsilon}_{rot}$ and $\hat{\varepsilon}_{vib}$, in Equations 4.1.7 and 4.1.11 are the basis for the internal distribution functions.

4.2 Larsen Borgnakke Method for Inelastic Collisions

As mentioned before, we are only considering inelastic collisions that exchange translational and either rotational or vibrational energy (there is no exchange between all three at once; see Section 3.3). So to abbreviate this method, we will refer to either rotational or vibrational energy simply as internal energy, $\hat{\varepsilon}_{int}$. Where necessary, we will specify what type of energy it is, either $\hat{\varepsilon}_{int_{rot}} = \hat{\varepsilon}_{rot}$ or $\hat{\varepsilon}_{int_{vib}} = \hat{\varepsilon}_{vib}$. Note that we are using scaled values of the internal energy here. The total energy of the collision is therefore,

$$\hat{\varepsilon}_c = \hat{\varepsilon}_{tr} + \hat{\varepsilon}_{int_{rot}} + \hat{\varepsilon}_{int_{vib}} , \quad (4.2.1)$$

with the definitions in a given collision:

$$\hat{\varepsilon}_{tr} = \frac{1}{4}(\beta\hat{g})^2 , \quad (4.2.2)$$

$$\hat{\varepsilon}_{int_{rot}} = \hat{\varepsilon}_{rot}(\hat{\zeta}) + \hat{\varepsilon}_{rot}(\hat{\eta}) , \quad (4.2.3)$$

$$\hat{\varepsilon}_{int_{vib}} = \hat{\varepsilon}_{vib}(\hat{\zeta}) + \hat{\varepsilon}_{vib}(\hat{\eta}) . \quad (4.2.4)$$

We recall that $\hat{\zeta}$ and $\hat{\eta}$ are the pre-collision velocity grid points. Also, we have arrived at our definition for $\hat{\varepsilon}_{tr}$ in much the same way as the procedure defined in Section 4.1.1. The definition for the kinetic energy of a collision on a per molecule basis is:

$$E_{tr} = \frac{1}{2} m^* g^2 . \quad (4.2.5)$$

Since velocities $\hat{\zeta}_i = (u_1, v_1, w_1)$ and $\hat{\eta}_i = (u_2, v_2, w_2)$ lie on the grid, they are restricted to integer values for their velocity components. Therefore the definition of g on the discrete grid, with indices i, j, k , is given by

$$g = \sqrt{(u_1 - u_2)^2 + (v_1 - v_2)^2 + (w_1 - w_2)^2} , \quad (4.2.6)$$

$$g = \sqrt{(\Delta\eta)^2(i_1 - i_2)^2 + (\Delta\eta)^2(j_1 - j_2)^2 + (\Delta\eta)^2(k_1 - k_2)^2} , \quad (4.2.7)$$

where if $\Delta\eta$ is uniform, we can consolidate g into:

$$g = \Delta\eta \sqrt{(i_1 - i_2)^2 + (j_1 - j_2)^2 + (k_1 - k_2)^2} . \quad (4.2.8)$$

We nondimensionalize the equation using $\beta = \frac{\Delta\eta}{\eta_r}$ to obtain:

$$\hat{g} = \frac{g}{\eta_r} = \beta \sqrt{(i_1 - i_2)^2 + (j_1 - j_2)^2 + (k_1 - k_2)^2} . \quad (4.2.9)$$

For colliding molecules of the same species, we realize that the reduced mass $m^* = \frac{m_1 m_2}{m_1 + m_2}$ becomes $m^* = m/2$. Our equation for translational energy per collision is:

$$E_{tr} = \frac{m}{4}(\eta_r \hat{g})^2 . \quad (4.2.10)$$

However in our code, \hat{g} is defined without β as

$$\hat{g} = \sqrt{(i_1 - i_2)^2 + (j_1 - j_2)^2 + (k_1 - k_2)^2} . \quad (4.2.11)$$

So our expression for translational energy must reflect this. Therefore, we have the specific translational energy per collision:

$$\varepsilon_{tr} = \frac{E_{tr}}{m} = \frac{1}{4}(\eta_r \beta \hat{g})^2 . \quad (4.2.12)$$

Dividing through by η_r^2 , we arrive at the scaled specific translational energy per collision seen in Equation 4.2.2. In the Larsen Borgnakke inelastic collision routine, we choose an arbitrary post collision translational energy ($\hat{\varepsilon}_{tr}'$) from 0 to $\hat{\varepsilon}_c$ and then consequently the rest of the energy goes to $\hat{\varepsilon}_{int}'$.

$$\hat{\varepsilon}_{tr}' = R_f \hat{\varepsilon}_c , \quad (4.2.13)$$

$$\hat{\varepsilon}_{int}' = \hat{\varepsilon}_c - \hat{\varepsilon}_{tr}' . \quad (4.2.14)$$

This value of $\hat{\varepsilon}_{tr}'$ is accepted if the ratio of probabilities $P(\hat{\varepsilon}_{tr}')/P_{max}$ (Equation 4.2.15) is greater than a second random number, R_f . (We obtain this ratio of probabilities from Bird [5] employing the Larsen Borgnakke method.) If not, we select a new $\hat{\varepsilon}_{tr}'$ using Equation 4.2.13 and we test the probability ratio again. This

acceptance rejection routine is repeated until we have a post collision $\hat{\varepsilon}_{tr}$ that passes.

The probability ratio for this selection is:

$$\frac{P(\hat{\varepsilon}_{tr}')}{P_{max}} = \left\{ \frac{\xi + \frac{1}{2} - \omega}{\frac{3}{2} - \omega} \left(\frac{\hat{\varepsilon}_{tr}'}{\hat{\varepsilon}_c} \right) \right\}^{3/2-\omega} \left\{ \frac{\xi + \frac{1}{2} - \omega}{\xi - 1} \left(1 - \frac{\hat{\varepsilon}_{tr}'}{\hat{\varepsilon}_c} \right) \right\}^{\xi-1}. \quad (4.2.15)$$

Here ξ is the number of internal degrees of freedom and ω is the viscosity temperature coefficient we discussed in Section 3.2.3 for the VHS technique. Next we assign new internal energies for post collision velocity points $\hat{\zeta}'$ and $\hat{\eta}'$. We choose one internal energy value to be arbitrary between 0 and $\hat{\varepsilon}_{int}'$ and the other is the remainder of $\hat{\varepsilon}_{int}'$.

$$\hat{\varepsilon}_{int}(\hat{\zeta}') = R_f \hat{\varepsilon}_{int}', \quad (4.2.16)$$

$$\hat{\varepsilon}_{int}(\hat{\eta}') = \hat{\varepsilon}_{int}' - \hat{\varepsilon}_{int}(\hat{\zeta}'). \quad (4.2.17)$$

Similar to the selection of $\hat{\varepsilon}_{tr}'$, the selection of $\hat{\varepsilon}_{int}(\hat{\zeta}')$ must also pass through an acceptance rejection routine. The probability ratio, as defined by Bird [5], for this selection is below, and must be greater than a second random number, R_f for $\hat{\varepsilon}_{int}(\hat{\zeta}')$ to be selected.

$$\frac{P(\hat{\varepsilon}_{int}(\hat{\zeta}'))}{P_{max}} = 2^{\xi-2} \left(\frac{\hat{\varepsilon}_{int}(\hat{\zeta}')}{\hat{\varepsilon}_{int}'} \right)^{\xi/2-1} \left(1 - \frac{\hat{\varepsilon}_{int}(\hat{\zeta}')}{\hat{\varepsilon}_{int}'} \right)^{\xi/2-1}. \quad (4.2.18)$$

Finally, we then shrink or grow the relative velocity vector according to the following equation:

$$\hat{g}' = \frac{\sqrt{4\hat{\epsilon}_{tr}'}}{\beta} . \quad (4.2.19)$$

The new relative velocity vector g' then replaces g and is used to find the two replenishing points. Since the post collision velocities $\hat{\zeta}'$ and $\hat{\eta}'$ can lie off the grid, so too can their assigned internal energies. The internal energy interpolation routine discussed in Section 4.3.3 follows the general procedure of the mass interpolation scheme discussed in Section 2.2.1 and can remap the internal energy back on the discrete velocity grid while conserving mass, momentum and energy.

4.3 New Method for Inelastic Collisions

The new method developed by Dr. Philip Varghese and myself for inelastic collisions borrows several redeeming qualities from the Larsen Borgnakke method, but offers improvements in representing the relationship between internal energy and translational energy. This method employs the general Landau-Teller equation format (see Section 3.3.3), but several adaptations are made. The last part of this section contains two important considerations: a description of how this new method must be adapted to work for the equilibrium collision integral in our variance reduction method, and the internal energy interpolation scheme that is employed to conserve energy and obtain the proper relaxation rate.

4.3.1 The Method

For this section, the discussion will assume rotational energy is the only form of internal energy. If we look at the gas contained in a cell, we know the behavior of

the gas as a whole. Or more precisely, using the Landau-Teller equation, we know how the rotational energy will change each sufficiently small time step with respect to a difference between the total rotational temperature (\hat{T}_{rot}) and the total translational temperature (\hat{T}_{tr}). We represent this relation as:

$$\Delta \hat{\varepsilon}_{rot} = \frac{d\hat{\varepsilon}_{rot}}{dt} \Delta t = \frac{\hat{\varepsilon}_{rot}(\hat{T}_{tr}) - \hat{\varepsilon}_{rot}(\hat{T}_{rot})}{Z_{rot} \tau_{coll}} \Delta t . \quad (4.3.1)$$

Recall that Z_{rot} is derived from the rotational relaxation rate; it is the number that determines fraction of collisions where an exchange of rotational energy occurs, and τ_{coll} is the collision time. Our representation for rotational energy is $\hat{\varepsilon}_{rot} = \hat{T}_{rot}/2$. Therefore, using this definition and the definition of scaled collision time $\delta \hat{t} = \Delta t / \tau_{coll}$, we have the equation for the total exchange of rotational and translational energy per time step:

$$\Delta \hat{\varepsilon}_{rot} = -\Delta \hat{\varepsilon}_{tr} = \frac{\hat{T}_{tr} - \hat{T}_{rot}}{2 Z_{rot}} \delta \hat{t} . \quad (4.3.2)$$

Recall that this is the the Landau-Teller equation we discussed in Section 3.3.3, but reduced to describe the change in rotational energy for one time step. If we wanted to remove the collision aspect of internal energy exchange that is present in the Larsen Borgnakke method, we could simply use this definition to model a bulk energy exchange each time step. This would accurately describe the relaxation of the independent energies as an equilibration of the total temperatures. (It is accurate to the extent that our choice of Z_{rot} is accurate and our scaled time step is small enough.) However, this would diminish the usefulness of the code especially when convection of

internal energy was required. For example, in a shock, only using the total rotational temperature of the rotational energy distribution would remove any non-uniformity in the internal energy that may be following any specific discrete velocity class as it is being convected across physical cells.

Therefore, we wish to preserve the collision aspect, so this general method for describing the energy exchange per time step must be projected on the collision scale. There is no such thing as the translational temperature of individual particles (translational temperature is a function of a velocity distribution), so we choose to use the temperature of the entire distribution at the beginning of the time step (\hat{T}_{tr_1}). The collision partners (η and ζ) each have their own rotational temperatures. Therefore, we use the average rotational temperature of the collision pair ($\bar{\hat{T}}_{rot}$).

$$\Delta \hat{\epsilon}_{rot} = \frac{\hat{T}_{tr_1} - \bar{\hat{T}}_{rot}}{2 Z_{rot}} \delta \hat{t} , \quad (4.3.3)$$

where,

$$\bar{\hat{T}}_{rot} = \frac{1}{2} \left(\hat{T}_{rot_\eta} + \hat{T}_{rot_\zeta} \right) . \quad (4.3.4)$$

We could instead write Equation 4.3.3 in terms of the translational energy for the collision. We begin by equating the translational energy per molecule and the translational energy of a molecule in a collision.

$$\frac{3}{2}kT_{tr} = \frac{1}{2}m^*(\beta g)^2, \quad (4.3.5)$$

$$\frac{3}{4}(2kT_{ref})\hat{T}_{tr} = \frac{1}{4}m(\beta\eta_r\hat{g})^2, \quad (4.3.6)$$

$$3\hat{T}_{tr} \left(\frac{2kT_{ref}}{m} \right) = \eta_r^2 (\beta\hat{g})^2. \quad (4.3.7)$$

We make use of the reference velocity $\eta_r = \left(\frac{2kT_{ref}}{m} \right)^{1/2}$ and solve for \hat{T}_{tr} to obtain:

$$\hat{T}_{tr} = \frac{1}{3}(\beta\hat{g})^2. \quad (4.3.8)$$

Since we define the first term in the Landau-Teller equation to be $\hat{\varepsilon}_{rot}(\hat{T}_{tr}) = \hat{T}_{tr}/2$, we obtain the following equation for an inelastic collision using the collision energy:

$$\Delta\hat{\varepsilon}_{rot} = -\Delta\hat{\varepsilon}_{tr} = \frac{\frac{1}{3}(\beta\hat{g})^2 - \hat{T}_{rot}}{2 Z_{rot}} \delta\hat{t}. \quad (4.3.9)$$

We may use either Equation 4.3.9 or Equation 4.3.3 to describe the energy exchange within inelastic collision; however, since we seek to keep the energy exchange on a per collision basis, Equation 4.3.9 is preferred. We will examine the difference between using the two options for translational temperature of the collision in Section 5.1.

One important thing to note here is that we have moved away from exchanging internal energy every Z_{rot} collisions. Instead, we now exchange internal and translational energy during every collision, except the amount exchanged is reduced by

the factor $\frac{1}{Z_{rot}}$. Therefore, the energy exchanged is less for each collision, but it is exchanged every collision, perhaps making the distribution smoother.

This change in rotational energy is associated with an equal and opposite change in translational energy, as seen in Equation 4.3.2. Given the original relative velocity vector (g), next we calculate the new relative velocity vector according to the change in internal energy. We begin with the definition of $\Delta\hat{\epsilon}_{tr}$:

$$\Delta\hat{\epsilon}_{tr} = \frac{1}{4}(\beta\hat{g}')^2 - \frac{1}{4}(\beta\hat{g})^2 . \quad (4.3.10)$$

Reorganizing and using the definition $\Delta\hat{\epsilon}_{rot} = -\Delta\hat{\epsilon}_{tr}$, we obtain the expression for g' :

$$\hat{g}' = \sqrt{\hat{g}^2 - \frac{4\Delta\hat{\epsilon}_{rot}}{\beta^2}} . \quad (4.3.11)$$

The last requirement of the collision is to update the rotational energy of the particles. Let us deal with the pre-collision velocity points first. We know that internal energy must have been removed (or added depending on the sign of mass being depleted) from the pre-collision velocity ζ and/or η . Both pre-collision points contribute $\delta\hat{E}_{rot} = \hat{\epsilon}_{rot}m_f$ to the collision. (This does not hold if multiple species are allowed and an atom collides with a diatomic molecule.) Here $\hat{\epsilon}_{rot_\zeta}$ is the scaled specific rotational energy of pre-collision velocity ζ and m_{f_ζ} is the mass depleted from point ζ . We can now determine how much scaled specific internal energy is left at pre-collision points ζ and η . (Note that we only have to look at one velocity point since the change at the other pre-collision point will be the same.)

$$\begin{aligned}
\hat{E}'_{rot_\zeta} &= \hat{E}_{rot_\zeta} - \delta \hat{E}_{rot_\zeta} , \\
\hat{\varepsilon}'_{rot_\zeta}(\hat{\varphi}_\zeta - m_{f_\zeta}) &= \hat{\varepsilon}_{rot_\zeta} \hat{\varphi}_\zeta - \hat{\varepsilon}_{rot_\zeta} m_{f_\zeta} , \\
\hat{\varepsilon}'_{rot_\zeta}(\hat{\varphi}_\zeta - m_{f_\zeta}) &= \hat{\varepsilon}_{rot_\zeta}(\hat{\varphi}_\zeta - m_{f_\zeta}) , \\
\hat{\varepsilon}'_{rot_\zeta} &= \hat{\varepsilon}_{rot_\zeta} .
\end{aligned} \tag{4.3.12}$$

The total change in rotational energy (\hat{E}_{rot}) is only due to the change in mass at the two pre-collision points. Therefore, the rotational energy per unit mass ($\hat{\varepsilon}_{rot}$) at the pre-collision velocity points does not change.

The post-collision velocity points are more interesting. These must also include the change in rotational energy $\Delta \hat{\varepsilon}_{rot}$ from translational energy. We once again put the scaled specific rotational energy, $\hat{\varepsilon}_{rot_\zeta}$ in terms of scaled rotational energy $\hat{E}_{rot_\zeta} = \hat{\varepsilon}_{rot_\zeta} \hat{\varphi}_\zeta$. Here, as before, we only need to examine one post-collision velocity; therefore, we choose velocity point ζ' .

$$\hat{E}_{rot_{\zeta \rightarrow \zeta'}} = \hat{E}_{rot_\zeta} + \frac{1}{2} \Delta \hat{E}_{rot} , \tag{4.3.13}$$

$$\hat{E}'_{rot_{\zeta'}} = \hat{E}_{rot_{\zeta'}} + \hat{E}_{rot_{\zeta \rightarrow \zeta'}} . \tag{4.3.14}$$

Here $\hat{E}_{rot_{\zeta \rightarrow \zeta'}}$ is the rotational energy taken from point ζ and given to point ζ' . However, it also contains the contribution from the inelastic collision, $\Delta \hat{E}_{rot}$. If we expand out the equation for one point ζ' , we can find $\hat{\varepsilon}'_{rot_{\zeta'}}$:

$$\begin{aligned}
\hat{\varepsilon}'_{rot_{\zeta'}}(\hat{\varphi}_{\zeta'} + m_{f_{\zeta}}) &= \hat{\varepsilon}_{rot_{\zeta'}}\hat{\varphi}_{\zeta'} + \hat{\varepsilon}_{rot_{\zeta \rightarrow \zeta'}}m_{f_{\zeta}} , \\
\hat{\varepsilon}'_{rot_{\zeta'}} &= \frac{\hat{\varepsilon}_{rot_{\zeta'}}\hat{\varphi}_{\zeta'} + \hat{\varepsilon}_{rot_{\zeta \rightarrow \zeta'}}m_{f_{\zeta}}}{\hat{\varphi}_{\zeta'} + m_{f_{\zeta}}} .
\end{aligned} \tag{4.3.15}$$

4.3.2 Special Accommodation for Variance Reduction

Section 2.2.2 discusses splitting the collision integral (\int_C) into separate parts: a collision integral that calculates equilibrium to equilibrium collisions (\int_{MB-MB}), one that calculates equilibrium to non-equilibrium collisions ($\int_{MB-\delta}$) and one that calculates non-equilibrium to non-equilibrium collisions ($\int_{\delta-\delta}$). Here the equilibrium distribution is the Maxwellian Boltzmann (represented by MB) and the non-equilibrium distribution is the deviation (represented by δ). We show this relationship below.

$$\int_C = \int_{MB-MB} + \int_{MB-\delta} + \int_{\delta-\delta} . \tag{4.3.16}$$

In variance reduction without internal energy, the integral, \int_{MB-MB} , is identically zero since collisions between equilibrium distributions, or identical Maxwellian distributions do not change the distribution function. However with the inclusion of internal energy, these equilibrium collisions must be accounted for since we know that all collisions are exchanging internal and translational energy for every time step. We will continue this discussion only for rotational energy, but it should be noted that vibration follows the same method.

Recall that we already derived the total energy exchange per time step in Section 4.3.1, Equation 4.3.2. We also know the expression for the scaled rotational

and translational energy per molecule per unit mass from Sections 3.1.3.2 and 3.1.2.

Using these definitions we can find the total change in temperature for \int_{MB-MB} .

$$\Delta \hat{T}_{rot} = 2\Delta \hat{\varepsilon}_{rot} \frac{N_{MB-MB}}{N_{tot}} , \quad (4.3.17)$$

$$(\Delta \hat{T}_{tr})_{rot} = \frac{4}{3} (\Delta \hat{\varepsilon}_{tr})_{rot} \frac{N_{MB-MB}}{N_{tot}} . \quad (4.3.18)$$

Here $(\Delta \hat{T}_{tr})_{rot}$ is the change in translational temperature due to rotation and N_{tot} is the number of total collisions for that time step. This is found by summing the total number of collisions for all the integrals: $N_{tot} = N_{MB-MB} + N_{MB-\delta} + N_{\delta-\delta}$. $N_{MB-\delta}$ and $N_{\delta-\delta}$ are calculated by Equations 2.2.5 and 2.2.7 respectively, and N_{MB-MB} is the number of collisions for \int_{MB-MB} , defined as:

$$N_{MB-MB} = nint \left(\frac{\Delta \hat{t} \hat{n}^2}{2 RMS^2} \right) \frac{\hat{T}_t^{(2/3)}}{\beta^3} . \quad (4.3.19)$$

To update the rotational energy distribution for this integral, we perform the following operation:

$$\hat{\varepsilon}'_{rot_i} = \hat{\varepsilon}_{rot_i} + \Delta \hat{\varepsilon}_{rot} \frac{N_{MB-MB}}{N_{tot}} . \quad (4.3.20)$$

This holds because no net mass is being exchanged point-wise for \int_{MB-MB} , so everywhere that has mass is gaining the fraction of rotational energy change for that integral. Lastly, \hat{T}_{tr_1} is known from the beginning of the time step, so \hat{T}_{tr_2} can be calculated by the following formula:

$$\hat{T}_{tr_2} = \hat{T}_{tr_1} + \frac{4}{3} \Delta \hat{\epsilon}_{tr} \frac{N_{MB-MB}}{N_{tot}} . \quad (4.3.21)$$

Recall that $\Delta \hat{\epsilon}_{tr} = -\Delta \hat{\epsilon}_{rot}$ so energy is conserved. With \hat{T}_{tr_2} , we can now compute the change in the Maxwellian distribution $\Delta \varphi_{MB}$. For consistency, the replenishing and depleting functions are updated as follows:

$$\Delta \hat{\varphi}_{repl_i} = \Delta \hat{\varphi}_{repl_i} + \hat{\varphi}_{MB_i}(\hat{T}_{tr_2}) , \quad (4.3.22)$$

$$\Delta \hat{\varphi}_{depl_i} = \Delta \hat{\varphi}_{depl_i} - \hat{\varphi}_{MB_i}(\hat{T}_{tr_1}) . \quad (4.3.23)$$

Therefore, when the replenishing and depleting functions are added to $\hat{\varphi}$ at the end of the time step, the change in the Maxwellian $\Delta \hat{\varphi}_{MB} = \hat{\varphi}_{MB}(\hat{T}_{tr_2}) - \hat{\varphi}_{MB}(\hat{T}_{tr_1})$ is also added.

4.3.3 Internal Energy Interpolation Scheme

The interpolation scheme for the velocity distribution has five constraints, the mass, momentum in the x, y and z directions and kinetic energy must be conserved. The only constraint for an internal energy interpolation scheme is that the total internal energy being remapped must be conserved, and internal energy must always be positive. However since the total internal energy is a function of the mass at a point, $\hat{E}_{int_i} = \hat{\epsilon}_{int_i} \hat{\varphi}_i$, we cannot simply map all the internal energy to one point and be done. In order to preserve energy through time steps, the amount of internal energy \hat{E}_{int} that gets mapped to a point in the internal energy distribution must have the same mass that gets mapped to the same point in the velocity distribution.

Since, the specific internal energy update for a point follows Equation 4.3.15, the consequent value of $\hat{\varepsilon}'_{rot_{\zeta'}}$ is dependent on the amount of mass moved to that point. Therefore, when the mass in the velocity interpolation is split into several parts, the true value of the specific internal energy at a point is dependent on the actual amount of mass given to that point. Therefore, the internal energy must follow all the mass fractions generated by the mass interpolation scheme. The mass conservation equation for all the mass fractions $(m_{fo}, m_{fix}, m_{fex}, \dots)$ of the original replenishing mass, m_{repl} , is given below:

$$m_{repl} = m_{fo} + m_{fix} + m_{fex} + m_{fiy} + m_{fey} + m_{fiz} + m_{fez} \quad (4.3.24)$$

Here a mass fraction m_f is defined as the replenishing mass multiplied by a fraction generated in Equation 2.2.1. These fractions can be negative, as is often the case for the external points, which have negative mass to counteract the increase in kinetic energy associated with splitting a positive replenishing mass among several velocity points. Furthermore, the replenishing mass can also be negative depending on whether or not the mass is removed from a negative section of the non-equilibrium distribution function, $\hat{\varphi}^d$, seen in Section 2.2.2. Lastly, the value of φ at the velocity point we desire to map internal energy to can also be negative, since negatives in the wings of the velocity distribution due to mass interpolation can accumulate over several time steps. These are often not large ($O(10^{-5})$ where the largest spikes are $O(10^{-1})$) and will be returned to a positive value after more collisions over several time steps map mass to the point. Note, that these negative values are not a concern

for the mass interpolation we use for the velocity distribution, since the update to a point is simply an addition or subtraction of a constant. The only reason these negatives are a concern for internal energy is because we employ Equation 4.3.15 to update the specific internal energy at a point.

Ideally, the interpolation to a point operates with all positive values for mass; however, referencing our discussion in the previous paragraph, we know that at any time, three numbers can be negative: m_{repl} , $\hat{\varphi}_{\zeta'}$, and $f_{\zeta'}$. To account for these negatives, we take the sign of each: ς_m , ς_φ and ς_f , and replace the the three parameters of concern with their absolute value. Modifying Equation 4.3.15 so that it now describes the update for $\hat{\varepsilon}$ of one of the interpolation points on the stencil (see Figure 2.3) we have:

$$(\hat{\varepsilon}_{rot_{\zeta'}})' = \frac{\hat{\varepsilon}_{rot_{\zeta'}} |\hat{\varphi}_{\zeta'}| + (\hat{\varepsilon}_{rot_{\zeta}} + \frac{1}{2} \varsigma_m \varsigma_\varphi \varsigma_f \Delta \hat{\varepsilon}_{rot}) |m_{repl} f_{\zeta'}|}{|\hat{\varphi}_{\zeta'}| + |m_{repl} f_{\zeta'}|} \quad (4.3.25)$$

The change in internal energy of a given post-collision mass is only be recorded as a change in the specific internal energy. Therefore, the negative additions to the equation are accounted for in the replenishing mass term. Figure 4.2 on the following page helps to illustrate the several possible cases for interpolation to a post collision velocity. The cases involving negative values for $\hat{\varphi}_{\zeta'}$ are not shown.

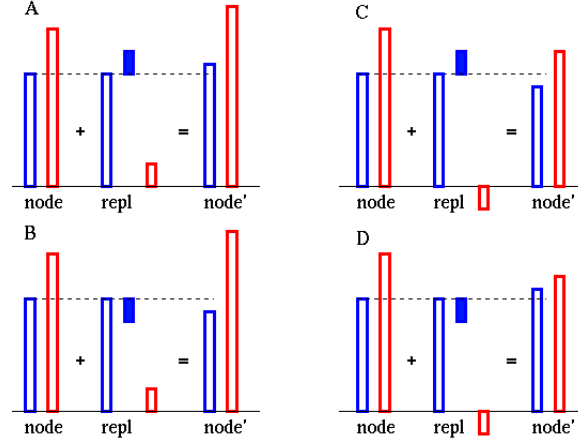


Figure 4.2: Shows four cases for positive and negative values of $\Delta\hat{\varepsilon}$ (the solid blue box) and positive and negative values of the replenishing mass fraction, m_f (the small red box). Above *node* and *node'*, the open blue boxes are values of the $\hat{\varepsilon}_{\zeta'}$ distribution, and the open red boxes represent the values of $\hat{\varphi}_{\zeta'}$. The open blue boxes above the *repl* represent the value of $\hat{\varepsilon}_{\zeta}$. Cases C & D have a negative m_f and Cases B & D have a negative $\Delta\hat{\varepsilon}$. The resulting value at point ζ' is seen above the *node'* label for each case. A is the ideal case where all values are positive.

Other interpolation methods we considered that do not use absolute values, must reject certain post-collision internal energies that display incorrect behavior when the difference in the denominator or numerator becomes very small and negative. The post-collision internal energy of such an interpolation can either explode to very large positive numbers or become negative, both of which are incorrect. Every collision that is rejected using a method like this slows the overall relaxation rate. Using the interpolation method in Equation 4.3.25 has the benefit that no collisions are rejected and the total energy of the system is conserved. Therefore, the internal energy and translational energy converge at the correct relaxation rate and the translational and rotational temperatures converge to the same equilibrium value.

Chapter 5

Results

The new method discussed in Section 4.3 is tested in this section and the results are discussed. We will begin with simple homogeneous relaxations of the rotational and translational distributions. Next, a one dimensional shock is examined using the same fourth order convection scheme discussed in [17], but modified to convect internal energy. Lastly, the results are compared to existing data for shock profiles with internal energy.

5.1 Homogeneous Relaxations

Physically, homogeneous relaxations are performed by heat bath simulations of particles with equilibrium rotational and translational distributions. To achieve a heat bath in experiments, a large quantity of inert gas like argon contains a small concentration of the diatomic species. Therefore, as the gas is held at a new temperature, the translational temperature of the system will equilibrate to the new temperature almost instantly, but the rotational temperature of the concentrated species will take longer to relax to equilibrium. Knowing the concentration of diatomic species, the relaxation rate can be calculated [25].

We simulate a related homogeneous relaxation by setting equilibrium transla-

tional and rotational distributions to different temperatures, then through collisions the distributions will exchange energy and arrive at an equilibrium temperature. For our simulations, we choose to run a case where the scaled rotational temperature, \hat{T}_{rot} , is set to 1 and the scaled translational temperature, \hat{T}_{tr} , set to 2. The scaled final temperature can be computed using conservation of energy and our scaling method:

$$\frac{3}{4}\hat{T}_{tr} + \frac{1}{2}\hat{T}_{rot} = \frac{3}{4}\hat{T}_{tr}' + \frac{1}{2}\hat{T}_{rot}' . \quad (5.1.1)$$

If we take the final time to be when the two temperatures are in equilibrium, then $\hat{T}_{final} = \hat{T}_{tr}' = \hat{T}_{rot}'$, and we can solve for \hat{T}_{final} :

$$\hat{T}_{final} = \frac{3}{5}\hat{T}_{tr} + \frac{1}{5}\hat{T}_{rot} . \quad (5.1.2)$$

Using this we expect a value of 1.6 given the set of initial temperatures we chose above. We choose to use pseudo-Maxwell molecules with a rotational relaxation collision constant, Z_{rot} , of 5. Figure 5.1 illustrates the homogeneous relaxation of rotational energy.

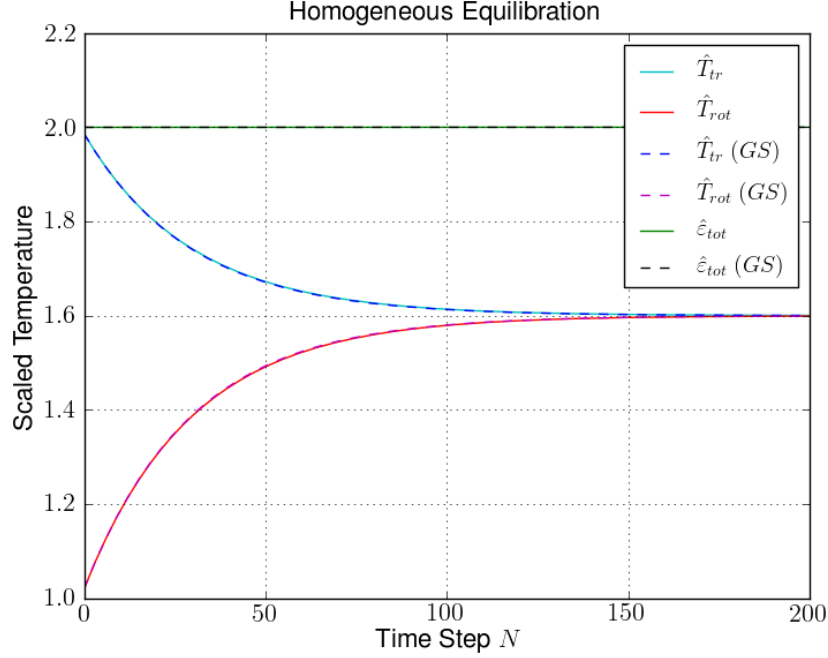


Figure 5.1: Temperature and energy profile for a homogeneous relaxation of rotational and translational energy for initial conditions of $\hat{T}_{rot} = 1$ and $\hat{T}_{tr} = 2$. The method of using the cell translational temperature to define the exchange of energy within the inelastic collision is used here (see Section 4.3.1).

The (GS) that denotes dashed lines stands for gold standard. The meaning of this is different than defined by Morris in [17]. Here gold standard refers to using the Landau-Teller equation to directly compute the total amount of energy transfer, $\Delta\hat{E}_{rot} = -\Delta\hat{E}_{tr}$, per time step. Therefore, the translational and rotational energy exchange that only happens during inelastic collisions is bundled into a total energy exchange for that time step. To account for the total translational and rotational energy exchange, the rotational energy and velocity distributions are only updated once per time step to have the new translational and rotational temperatures computed

by the Landau-Teller equation. The elastic component of a collision is preserved, and collisions still operate on the velocity distribution.

We observe in Figure 5.1 that the new method using the cell temperature matches the gold standard almost exactly. This is expected since this method is highly similar to the Landau-Teller equation that governs the gold standard. We now run the same case, but instead of the cell temperature, we use the collision energy (Equation 4.3.9).

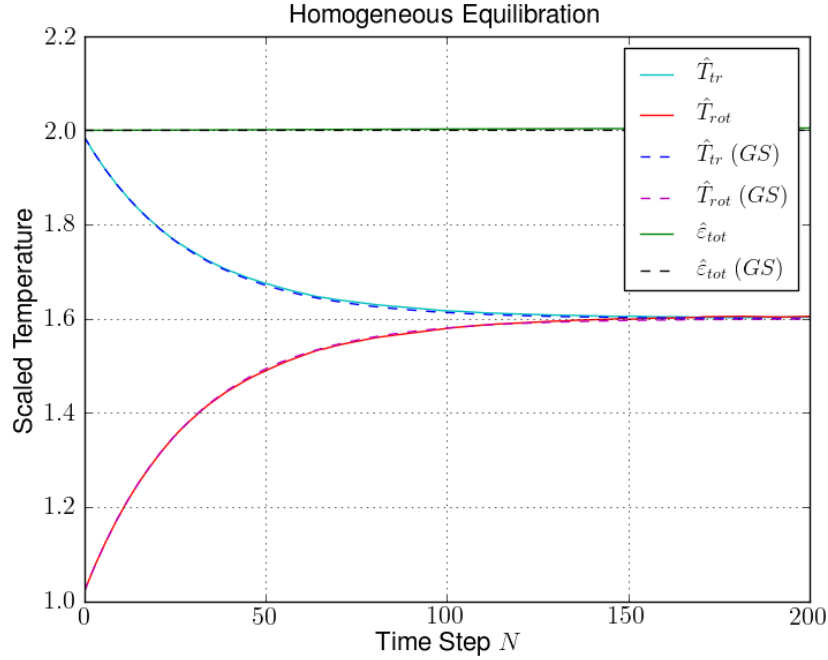


Figure 5.2: The same case as in Figure 5.1, but the collision energy is used here to define the translational temperature of the collision instead of the cell translational temperature. The scaled final temperature of translation and rotation matches the expected $\hat{T}_{final} = 1.6$ to within 0.5%.

In Figure 5.2, the new method using only the instantaneous collision energy

does not match the gold standard as exactly as using the cell temperature. We expect this since the collision energy is highly variable, and therefore the two options will produce the same result only in the limit as the number of collisions goes to infinity. We compare the error between the two methods in Figure 5.3.

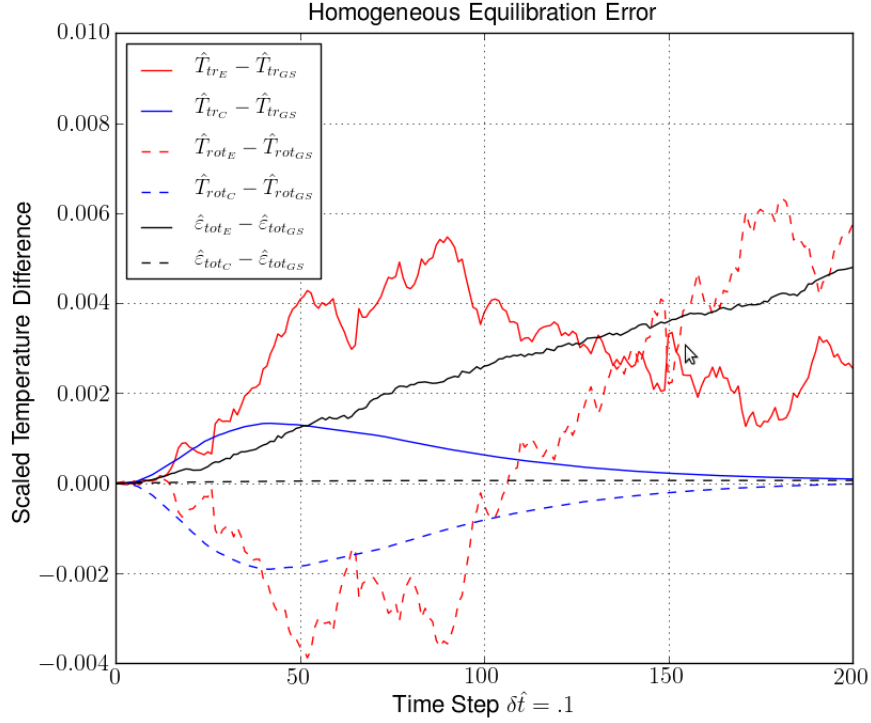


Figure 5.3: Error between the two options for translational temperature in the inelastic collision. Subscript C represents the cell temperature option used in Figure 5.1, and subscript E represents the collision energy option used in Figure 5.2.

We see that for the case where the cell temperature is used, the error in temperatures approaches zero as distributions reach the equilibrium temperature. However, when using the collision energy, the error in the temperatures does not

approach zero for the time-span shown. The method of using collision energy also experiences significantly more error than the other method. The biggest concern, however, is the monotonically increasing error in total energy. While the value is not large for 200 time steps, one could extrapolate this error as the number of time steps increases to the thousands. The cause of this error is currently under investigation. Lastly, we desire to compare the homogeneous solution obtained in Figure 5.2 with a DSMC homogeneous solution for a VHS parameter of $\omega = 0.75$ and the same rotational relaxation collision number, $Z_{rot} = 5$. Using data provided in Figure 11.2 of Bird [5], we can overlay the two data sets and obtain direct comparison.

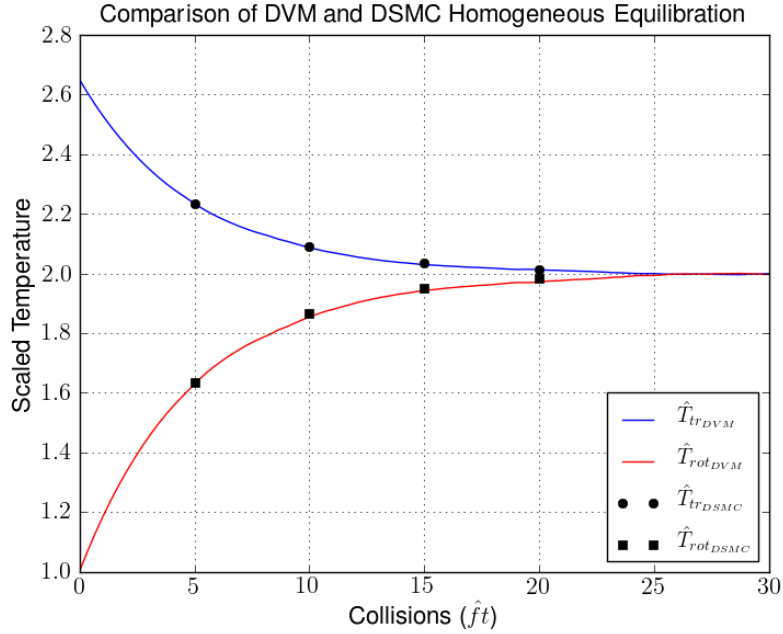


Figure 5.4: A comparison of the discrete velocity method (DVM) for solving the Boltzmann equation with rotational energy, and the direct simulation Monte Carlo (DSMC) method with rotational energy. $Z_{rot} = 5$ and the x-axis represents the number of equilibrium collisions described by the collision rate, \hat{f} , and the time, t .

The data sets converge as expected at the same Landau-Teller relaxation rate. To obtain the inelastic collision rate for the discrete velocity method in the same terms as DSMC, one must use the following equation:

$$\hat{f} = \hat{n} \hat{\sigma} \hat{g} \Lambda = \hat{n} \left(\frac{\sigma_o}{\sigma_{refDVM}} \right) \left(\frac{g_o}{\eta_r} \right) \left(\frac{1}{Z_{rot}} \right) \left(\frac{\sigma_{refDVM}}{\sigma_{refDSMC}} \right), \quad (5.1.3)$$

where Λ is defined as the fraction of total collisions that are inelastic, g_o is defined as η_r , so $\frac{g_o}{\eta_r} = 1$, and $\frac{\sigma_{refDVM}}{\sigma_{refDSMC}} = [2(2 - \omega)]^\omega$ as derived in Appendix A of Morris *et al.* [16]. Therefore, we obtain the collision rate to be:

$$\hat{f} = \frac{\hat{n}[2(2 - \omega)]^\omega}{Z_{rot}}. \quad (5.1.4)$$

For different gases modeled by the variable hard sphere collision model (i.e. the viscosity index, ω , is no longer 0.5 for pseudo-Maxwell molecules in DVM; 1.0 for pseudo-Maxwell molecules in Bird's homogeneous relaxation code, DSMC0R.F [5]), the rates can differ by as much as 5%. This can be seen in Figure 11.2 of Bird [5].

5.2 1D Normal Shock with Internal Energy

This section will discuss a one dimensional normal shock with internal energy as generated by the new method for incorporating internal energy in the framework of the discrete velocity method for solving the Boltzmann equation. The right traveling shock wave is formed by colliding left flowing gas into a specular wall. Knowing the upstream conditions, we can calculate the downstream conditions using the Rankine-Hugoniot relations. The assumptions for these relations are that the gas is calorically

perfect, 1-D and inviscid. The density, temperature and pressure relations are given below:

$$\frac{\hat{\rho}_2}{\hat{\rho}_1} = \frac{(\gamma+1)M^2}{(\gamma-1)M^2+2} , \quad (5.2.1)$$

$$\frac{\hat{T}_2}{\hat{T}_1} = [2 + (\gamma - 1)M^2] \frac{2\gamma M^2 - (\gamma - 1)}{(\gamma + 1)^2 M^2 + 2} , \quad (5.2.2)$$

$$\frac{\hat{p}_2}{\hat{p}_1} = [2\gamma M^2 - (\gamma - 1)] \frac{1}{\gamma + 1} . \quad (5.2.3)$$

Here, M is the shock's Mach number and γ is the ratio of specific heats defined as $\gamma = \frac{c_p}{c_v}$. The ratio of specific heats is also tied to the number of degrees of freedom, f , for the gas species. The number of degrees of freedom is dependent on the structure of the molecule and energy modes that are excited. This relation to degrees of freedom is given as,

$$\gamma = \frac{f + 2}{f} . \quad (5.2.4)$$

For species with no internal structure, the number of degrees of freedom is 3 (for the three translational directions) and the gas has $\gamma = 5/3$. If we introduce the two rotational degrees of freedom, $\gamma = 7/5$. This is the γ we proceed with since the only form of internal energy for these simulations is rotation.

The Rankine-Hugoniot relations in Equations 5.2.1 to 5.2.3 depend on the Mach number. Since the free-stream is not stationary, we need to compute the shock speed \hat{u}_s . This is performed taking the positive root of the following equation:

$$\hat{u}_s^2 - \frac{3-\gamma}{2}\hat{u}_1\hat{u}_s - \frac{1}{2}[\gamma + (\gamma-1)\hat{u}_1^2] = 0, \quad (5.2.5)$$

then, the Mach number can be computed by: $M = (\hat{u}_s - \hat{u}_1)\sqrt{2/\gamma}$. For the 1-D right traveling shock simulations performed below, the domain is initialized with a density: $\hat{n}_1 = 1$, temperature: $\hat{T}_{tr1} = \hat{T}_{rot1} = 1$, and an x velocity of $\hat{u}_1 = -1$. These conditions produce a Mach 1.97 shock. For all the simulations, the velocity grid in each cell is uniform with 13 grid points in each direction (i.e. $i_{max} = 6$, $i_{min} = -6$) and a velocity grid spacing of $\beta = 0.7$.

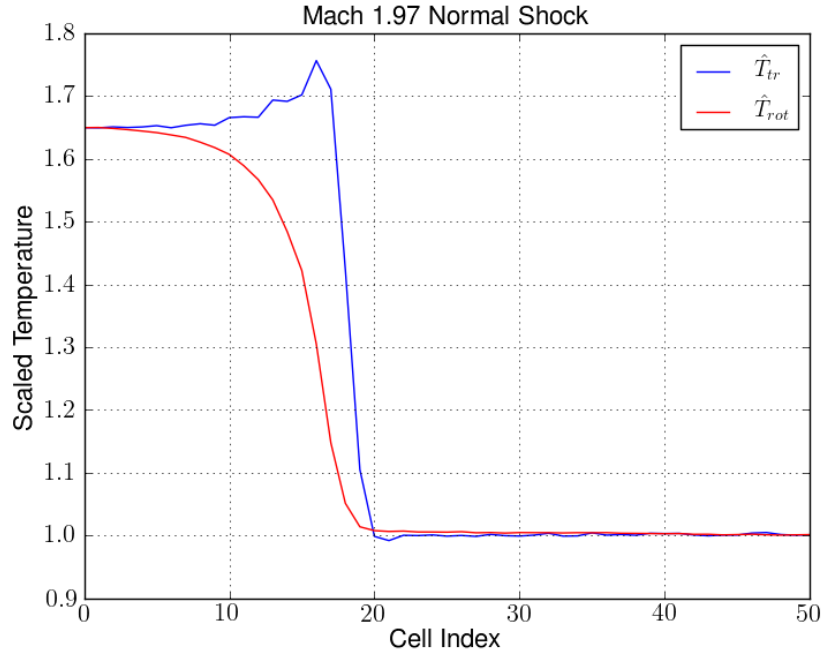


Figure 5.5: Rotational and translational temperature profiles for Mach 1.97 normal shock, performed with a physical spacing $a = \Delta x/\lambda_{up} = 1$ and scaled time step $\delta\hat{t} = 0.05$. λ_{up} is the upstream mean free path.

We calculate the expected downstream temperature using Equation 5.2.2 to be $\hat{T}_2 = 1.645$. We see that the simulated downstream temperature agrees with the Rankine-Hugoniot temperature to within 0.5%. The Mach 1.97 nitrogen shock is coarse due to the unrefined nature of the the physical spacing, a . If we refine in physical space and normalize according the following relation,

$$\hat{T}^* = \frac{\hat{T} - \hat{T}_{up}}{\hat{T}_{down} - \hat{T}_{up}}, \quad (5.2.6)$$

we arrive at the shock seen in Figure 5.6.

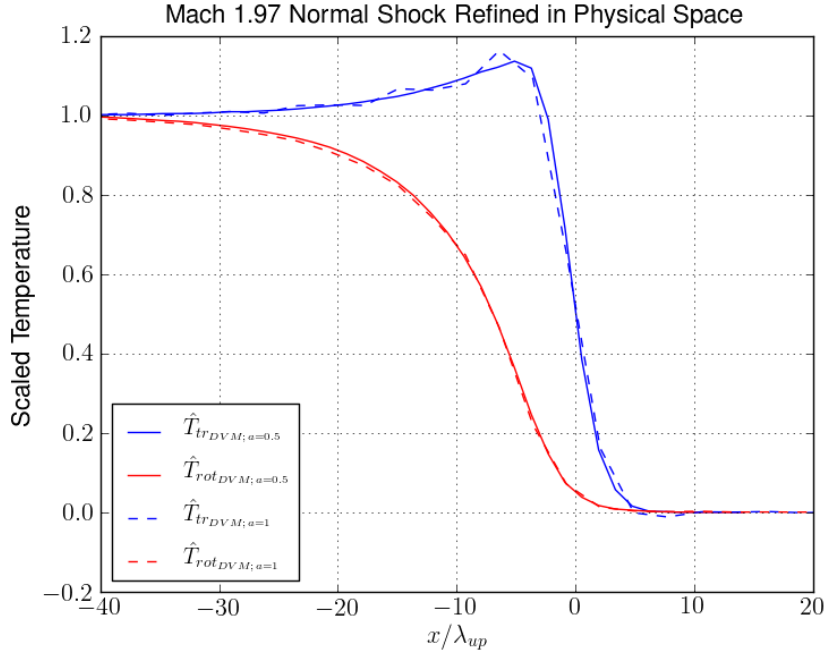


Figure 5.6: Comparison of Figure 5.5 with a spatially refined and normalized Mach 1.97 normal shock. This normal shock was performed with a physical spacing $a = \Delta x/\lambda_{up} = 0.5$ and scaled time step $\delta\hat{t} = 0.05$. The rotational relaxation collision constant is $Z_{rot} = 5$.

The hump that is visible in the translational temperature is produced by the slow transfer of energy into the internal modes; here, the only internal modes available are rotational. The height and breadth of the hump are dependent on the relaxation rate for the internal modes. With such a shock, we can easily compare to 1-D shock waves produced by other available rarefied gas dynamics solvers, particularly direct simulation Monte Carlo or DSMC [5]. This will be the focus of the following section.

5.3 Comparison to DSMC

DSMC incorporates internal energy by use of the the Larsen Borgnakke method of handling inelastic collisions discussed in Section 4.2. To allow a consistent comparison, we set the only form of internal energy to be rotation, and specify the same relaxation rate in both DVM and DSMC by setting $Z_{rot} = 5$ in both programs.

Furthermore, care must be taken to make sure the physical space is consistent. The systematic approach to this is to scale both sets of data by the upstream mean free path λ_{up} . Bird defines his mean free path in DSMC [5] to be:

$$\lambda_{up} = \frac{\left(\frac{T}{T_{ref}}\right)^\omega}{(2 - \omega)^\omega \Gamma(2 - \omega) \sqrt{2} n \sigma_{ref}} \quad (5.3.1)$$

The DVM λ_{up} must match Bird's in order to obtain meaningful results. Therefore we choose to multiply the DSMC physical length, x/λ_{up} , by $\lambda_{DSMC}/\lambda_{DVM}$, where it is implied that the mean free path is calculated for upstream conditions. This re-scaling essentially uses the parameter $\frac{\sigma_{refDVM}}{\sigma_{refDSMC}}$ as given in Section 5.2 and derived in Appendix A of Morris *et al.* [16]. As a check, we show that the temperature profile

for a monatomic gas is consistent (Figure 5.7 below).

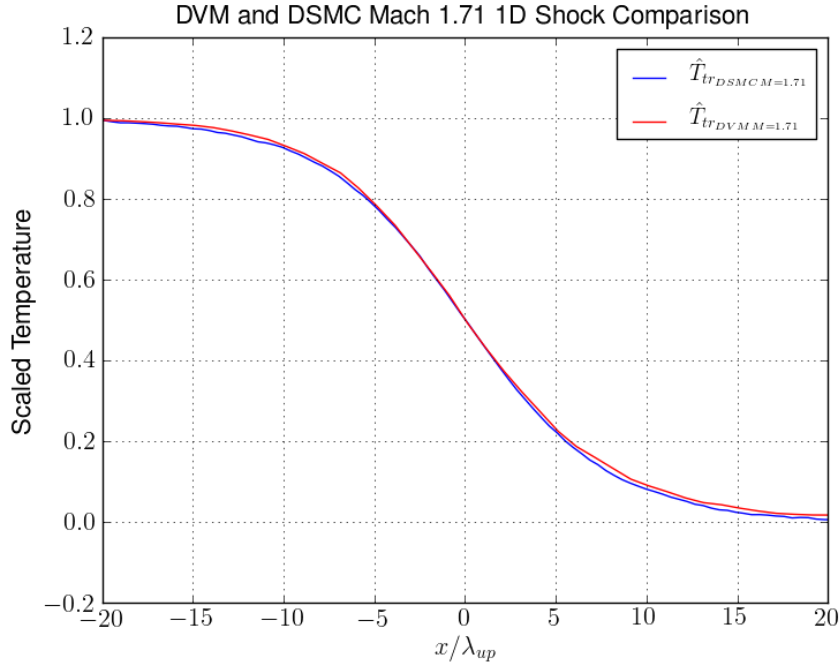


Figure 5.7: Normalized DSMC and DVM temperature profiles for Mach 1.71 monatomic normal shocks. Performed using pseudo-Maxwell molecules for both methods, and for the DVM shock, a uniform velocity space of 13^3 and a scaled velocity grid spacing of $\beta = 0.7$ is used. The physical spacing is $a = 0.5$ and the scaled time step is $\delta\hat{t} = 0.05$. The DSMC shock was obtained using the code DSMC1S.F [5].

Now we can proceed to the diatomic case with rotational energy. We first use pseudo-Maxwell molecules in both DSMC and DVM and compare the shock profiles. Using the same velocity and physical parameters listed in the caption of Figure 5.7, we compare the normalized DSMC temperature profiles with the normalized DVM temperature profiles for a Mach 1.71 normal shock with rotational energy.

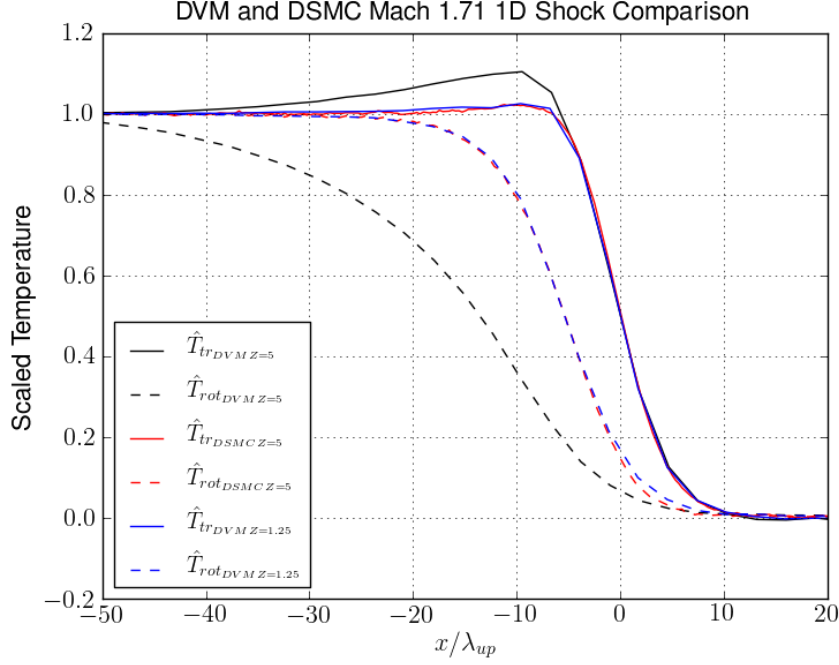


Figure 5.8: Normalized DSMC and DVM temperature profiles for a Mach 1.71 normal shock with rotational energy. The DSMC normal shock is simulated with a relaxation rate corresponding to $Z_{rot} = 5$, whereas for DVM, two cases—a relaxation rate $Z_{rot} = 5$ and 1.25—are shown.

Here, DSMC and both DVM temperature profiles meet the Rankine-Hugoniot conditions downstream for $\hat{T}_{final} = 1.585$ to within 0.5%. The primary difference between the two plots for $Z_{rot} = 5$ is that the DSMC rotational relaxation rate is much faster than the DVM rate. Consequently, the translational temperature for DSMC does not display the hump structure seen in the DVM translational temperature. The DVM normal shock with $Z_{rot} = 1.25$, however, illustrates the difference in relaxation rates by demonstrating a faster rate with the DVM method. We see in this plot that the DVM simulation for $Z_{rot} = 1.25$ has a translational and rotational

temperature profile that match the DSMC simulation for $Z_{rot} = 5$ almost precisely. The explanation for this factor of $\frac{1}{4}$ of Z_{rot} required to obtain a consistent rotational relaxation rate is unknown, but is under investigation currently.

Furthermore, we wish to examine a normal shock using the VHS and VSS parameters for nitrogen, ω_{N_2} and α_{N_2} respectively, in both programs. We demonstrate this in the figure below.

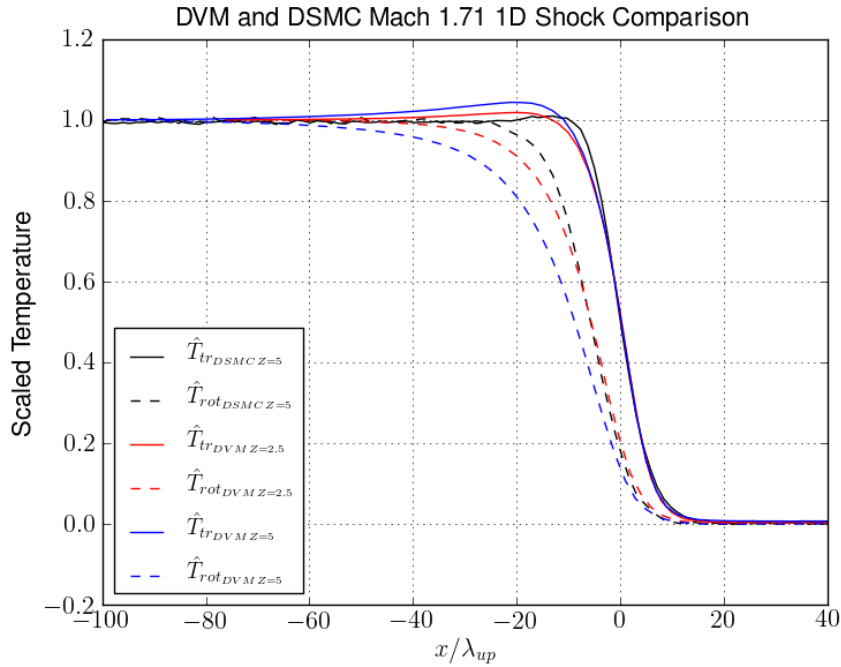


Figure 5.9: Normalized DSMC and DVM temperature profiles for Mach 1.71 normal shock using variable hard sphere and variable soft sphere parameters for nitrogen. The same configuration of physical and velocity space parameters were used as in Figure 5.7

Figure 5.9 shows both DVM translational temperature profiles agree well with the DSMC profile for the upstream half of the shock profile, but the downstream shock

thickness seems to expand before the DSMC shock. Furthermore, it is interesting that the DVM downstream translational temperature profiles seem to start relaxing before DSMC, yet still have a larger translational temperature hump. The variable hard sphere model was also employed without VSS and there was negligible difference for both of the DVM cases and the DSMC simulation.

Ultimately, we wish to know which method achieves the most accurate results. The best way to do this is to compare to experimental results like those obtained by Alsmeyer [2]. Another perhaps more revealing way to compare the two programs would be to implement Larsen Borgnakke inelastic collision approach in the DVM code and compare it to both DSMC and DVM using the new method for inelastic collisions. This too remains under development.

5.4 Convection and Velocity Grid Refinement

This section investigates the effect of refining the discrete velocity grid and using an alternative convection method on the normal shock profiles. We will begin with refining the discrete velocity grid.

In the previous DVM cases, the velocity grid in each cell was uniform with 13 grid points in each direction (i.e. $i_{max} = 6$, $i_{min} = -6$) and had a velocity grid spacing of $\beta = 0.7$. The same Mach 1.71 normal shock is now simulated using the discrete velocity method on a uniform velocity grid with 25 grid points in each direction (i.e. $i_{max} = 12$, $i_{min} = -12$) and a velocity grid spacing of $\beta = 0.35$. The other physical parameters remain the same: the physical spacing, $a = 0.5$, and the scaled time step, $\delta\hat{t} = 0.05$. Lastly, this was performed using VHS for nitrogen, $\omega_{N_2} = 0.74$, and a

rotational relaxation collision number of $Z_{rot} = 5$. The following plot is obtained.

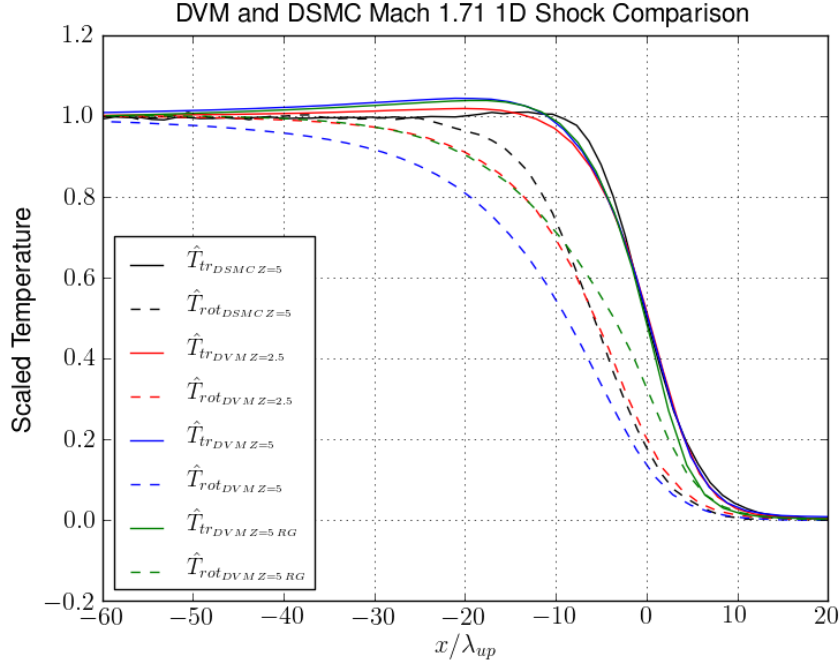


Figure 5.10: Normalized DSMC and DVM temperature profiles for Mach 1.71 normal shock using VHS for nitrogen. The refined grid is denoted by RG.

The results in Figure 5.10, show that the DVM normal shock with rotational energy is un-converged in velocity space. Further investigation is needed to determine why this is the case. Interestingly, the refined grid normal shock did not display any wall effects that are present in the unrefined grid simulations.

For all the preceding DVM normal shock simulations, a fourth order Runge-Kutta convection method has been used [17]. Here we desire to test the simple upwind first order scheme also implemented by Morris [17]. The parameters a and $\delta\hat{t}$ are kept the same as those used to generate Figure 5.10; however, here pseudo-Maxwell

molecules are used. Furthermore, this simulation is performed on the unrefined, 13^3 , uniform velocity grid with $\beta = 0.7$. The first order scheme for convection is compared to the fourth order scheme below.

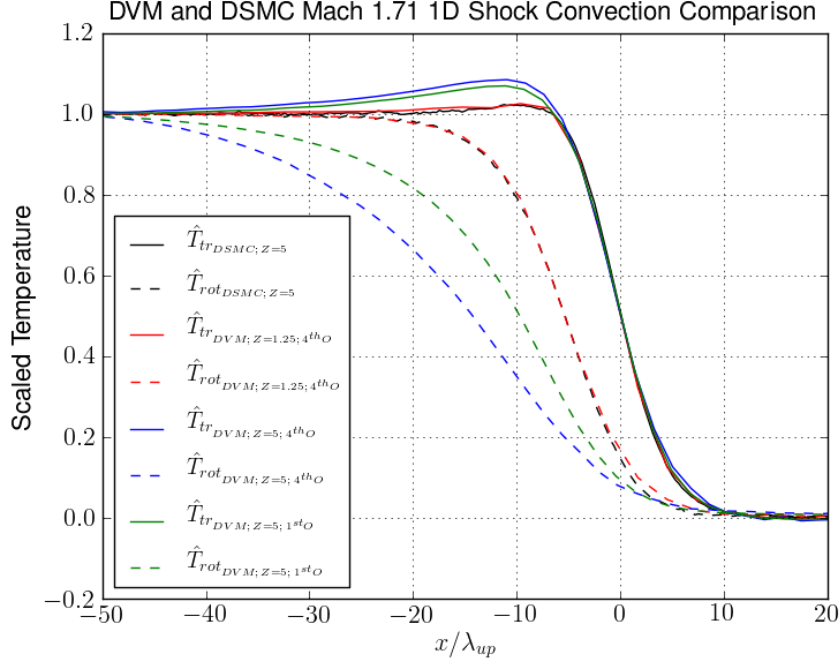


Figure 5.11: Normalized DSMC and DVM temperature profiles for Mach 1.71 normal shock using two different methods for convection.

The first order convection method with a $Z_{rot} = 5$ gives a faster relaxation rate than the fourth order convection method. However, these methods should not compute any difference in relaxation rate. This leads to the conclusion that errors in the convection of internal energy could be contributing factors to the unknown factor of $\frac{1}{4}$ difference in rotational relaxation collision constants seen in Figure 5.8. Further tests of the convection routine for internal energy are required.

Chapter 6

Conclusions

The objective at outset of this thesis was to develop the capacity to handle gases with internal energy within the framework of the existing discrete velocity Boltzmann equation solver, particularly in its most advanced form: the variance reduction method. Through the course of this paper, an outline of how to handle multiple modes of internal energy was presented, and rotational energy, represented by a single value instead of a distribution at each velocity point, was implemented. A new method was developed to represent the exchange of translational and internal energy. The method employed the Landau-Teller equation for the bulk translational and internal energy exchange to govern that energy exchange during inelastic collisions. An interpolation scheme was also developed in addition to the existing velocity interpolation scheme to handle post-collision internal energy re-distribution to the discrete velocity grid while continuing to preserve mass, momentum and total energy.

Homogeneous relaxations showed that for the zero dimensional case of a gas with an initial scaled translational temperature of 2 and an initial scaled rotational temperature of 1 the expected final temperature was met to within 0.5% error, and the correct relaxation rate according to the analytic Landau-Teller equation was shown. A comparison to the direct simulation Monte Carlo (DSMC) method showed that

the Discrete Velocity Method (DVM) homogeneous case relaxed at the same rate. The internal energy exchange method was next examined via the simulation of a one dimensional normal shock. For a Mach 1.97 normal shock, the new method was shown to meet the Rankine-Hugoniot downstream temperature for both translational and rotational temperature, again within 0.5% error. A Mach 1.71 normal shock with rotational energy was generated by the DSMC method and was compared to the shock profiles for a DVM normal shock of the same Mach number. The DSMC shock unexpectedly showed a faster rotational relaxation rate than the shock generated by the DVM.

In addition to the above primary developments, the Variable Hard Sphere and Variable Soft Sphere collision models were added to the probability distribution in the collision selection model. The Larsen Borgnakke Method for inelastic collisions was outlined and developed for the DVM Boltzmann equation solver, but remains to be tested. The method to incorporate vibrational energy was outlined and the framework was developed to allow for its implementation. Furthermore, the framework exists within the DVM Boltzmann equation solver to allow for the rotational and vibrational energy to be represented as a distribution at every node in velocity space.

6.1 Future Work

First, a couple of outstanding issues must be resolved. For the homogeneous case, the source of the monotonically increasing error need to be tracked down. This may play a role in some of the wall effects seen in the normal shock simulations. Another area of study is internal energy convection. Since the different convection

methods produce different rotational relaxation rates, an error in the first or fourth order convection routine may be the primary source of the difference in relaxation rates between the DVM and DSMC method. Furthermore, the refined velocity grid seems to be converging to the correct relaxation rate, but for unknown reason. More refined discrete velocity grid tests must be performed to understand this behavior. Lastly, the variable hard sphere and variable soft sphere collision models require further testing to accurately understand Figure 5.9. When these tests are complete, comparing both DSMC and the DVM to Alsmeyer’s experimental results [2] could illuminate which method is a more accurate representation of rotational energy in a normal shock.

One natural advancement of the internal energy method developed here for the discrete velocity Boltzmann equation solver would be to represent the rotational and vibrational energy as distributions at every velocity node. Particularly the vibrational energy distribution would benefit, since molecules at low temperatures are generally in the ground vibrational energy level. The rotational energy may ultimately be kept to a single level representation since the rotational relaxation rate is typically faster than vibrational.

An interesting opportunity exists within the DVM if molecular vibration is to be modeled. The vibrational energy level transitions for an anharmonic oscillator model of a specific species of gas can be pre-calculated and used to accurately describe an anharmonic vibrational model for inelastic collisions. Adamovich *et al.* accurately described the vibrational relaxation rate by using the forced harmonic oscillator model to find vibrational transition rate coefficients [1]. These rate coefficients

are computed analytically through thermal averaging of collision based transition probabilities. Boyd used these probabilities in DSMC to accurately characterize the vibrational relaxation [8]. However, the probabilities discussed here require complex calculation, so performing the calculation on the fly for a specific set of two velocities in a DSMC collision is impractical. Therefore, probabilities for a set of relative velocity bins are pre-calculated and a finite number of energy level transitions are allowed. In a discrete velocity approach, as in the Boltzmann equation solver discussed in this thesis, all the relative velocity values are known, so a table for the total distribution could be pre-computed and used without sorting relative velocities into bins. This is unlike Boyd’s modification for DSMC in [8], which allows for all possible relative velocities, and therefore, sorting an arbitrary collision’s relative velocity into a bin sacrifices the exactness of the transition probabilities.

Finally, inelastic collisions should be able to exchange translational energy and multiple forms of internal energy per collision. Electronic excitation can also be incorporated, but this framework is not yet written and requires development. Lastly, dissociation, ionization and the inclusion of multiple species complicates the problem significantly, but a competitive rarefied gas solver should incorporate such possibilities.

Bibliography

- [1] I. Adamovich, S. Macheret, J. Rich, and C. Treanor. Vibrational Energy Transfer Rates Using a Forced Harmonic Oscillator Model. *Journal of Thermodynamics and Heat Transfer*, 12, 1998.
- [2] H. Alsmeyer. Density Profiles in Argon and Nitrogen Shock Waves Measured by the Absorption of an Electron Beam. *Journal of Fluid Mechanics*, 74, 1976.
- [3] P. Bhatnagar, E. Gross, and M. Krook. Model for Collision Process in Gases, I. Small Amplitude Processes in Charged and Neutral One-Component Systems. *Physics Review*, 94, 1954.
- [4] G. A. Bird. “Definition of a Mean Free Path for Real Gasses”. *Physics of Fluids*, 26, 1983.
- [5] G. A. Bird. *Molecular Gas Dynamics and the Direct Simulation of Gas Flows*, volume 42 of *Oxford Engineering Sciences Series*. Clarendon Press, 1994.
- [6] C. Borgnakke and P. S. Larsen. Statistical Collision Model for Monte Carlo Simulation of a Polyatomic Gas Mixture. *Journal of Computational Physics*, 18, 1975.
- [7] Iain Boyd. Analysis of Vibrational-Dissociation-Recombination Processes Behind Strong Shock Waves of Nitrogen. *Physics of Fluids A*, 4, 1992.

- [8] Iain Boyd and Eswar Josyula. State Resolved Vibrational Relaxation Modeling for Strongly Nonequilibrium Flows. *Physics of Fluids*, 23, 2011.
- [9] Gerhard Herzberg. *Molecular Spectra and Atomic Structure. I. Spectra of Diatomic Molecules*. Van Nostrand Company Inc., 2nd edition, 1950.
- [10] K. Koura and H. Matsumoto. “Variable Soft Sphere Molecular Model for Inverse-Power-Law or Leonard-Jones Potential”. *Phys. Fluids A* 3, 10, 1991.
- [11] Max Krook and Tai Tsun Wu. “Exact Solutions of the Boltzmann Equation”. *Physics of Fluids*, 20(10), 1977.
- [12] L. Landau and E. Teller. Theory of Sound Dispersion. *Phys. Zeits. d. Sowjetunion*, 10, 1936.
- [13] R. Millikan and D. White. Systematics of Vibrational Relaxation. *Journal of Chemical Physics*, 39, 1963.
- [14] Charlotte E. Moore. *Atomic Energy Levels*, volume I, II, III. National Bureau Standards Circular, 1949, 1952, 1958.
- [15] A. Morris, P. Varghese, and D. Goldstein. Improvement of a Discrete Velocity Boltzmann Equation Solver that Allows for Arbitrary Post-Collision Velocities. *Rarefied Gas Dynamics: Proceedings of the 26th International Symposium*, Kyoto, Japan, 2010.
- [16] A. Morris, P. Varghese, and D. Goldstein. Monte Carlo Solution of the Boltzmann Equation Via a Discrete Velocity Model. *Journal of Computational Physics*, 230, 2011.

- [17] Aaron Morris. Monte Carlo Solution of the Boltzmann Equation Via a Discrete Velocity Model. Master's thesis, The University of Texas at Austin, 2010.
- [18] A. Nordsieck and B. Hicks. Monte Carlo Evaluation of the Boltzmann Collision Integral. *Proc. 5th International Symposium on Rarefied Gas Dynamics*, 1967.
- [19] Chul Park. Review of Chemical-Kinetic Problems of Future NASA Missions, I: Earth Sciences. *Journal of Thermophysics and Heat Transfer*, 7, 1993.
- [20] S. P. Popov and F. G. Tcheremissine. A Conservative Method for Solving the Boltzmann Equation with Centrally Symmetric Interaction Potentials. *Computational Math and Math Physics*, 39, 1999.
- [21] Z. Tan and P. Varghese. The Δ - ϵ Method for the Boltzmann Equation. *Journal of Computational Physics*, 110, 1994.
- [22] F. G. Tcheremissine. A Method for Direct Numerical Integration of the Boltzmann Equation. *Numerical Methods in the Theory of Gases*, Edited by V.P. Shidlovskii, Moscow: Comput. Cent., USSR Acad. Sci. Transl. in NASA TT F-638, 1969.
- [23] F. G. Tcheremissine. Direct Numerical Solution of the Boltzmann Equation. *Rarefied Gas Dynamics, AIP, Conference Proceedings*, NY, edited by M. Capitelli, 2005.
- [24] F. G. Tcheremissine. Solution of the Boltzmann Equation for High Speed Flows. *Computational Math and Math Physics*, 39, 2006.

- [25] Walter G. Vincenti and Charles H. Kruger Jr. *Introduction to Physical Gas Dynamics*. John Wiley and Sons, 1965.
- [26] S. M. Yen. Numerical Solution of the Nonlinear Boltzmann Equation for Non-Equilibrium Gas Flow Problems. *Annual Review Fluid Mechanics*, 16, 1984.

Vita

David Benjamin Hegermiller was born in Southampton, New York on May 8th, 1988, the son of Cheryl and David Hegermiller. He was followed by four siblings, Anna, Gilbert, Emma and Katherine. From 2002 to 2006, he attended Chaminade High School in Mineola, New York. From there he enrolled in Princeton University, where he majored in mechanical and aerospace engineering with a certificate in sustainable energy. Upon graduating from Princeton with his Bachelor of Science in Engineering in May, 2010, his project team consisting of himself, Trevor O'Neill and Nathan Buch, received the John Marshall II Memorial Prize for their design and construction of a solar powered drone aircraft. During the summer of 2010, the three members of the team founded Solair Technologies Inc. to continue work on the project. In the fall of 2010, David enrolled in the University of Texas at Austin in pursuit of his Master of Science in Engineering degree in aerospace engineering, focusing on the field of aerothermodynamics and fluid mechanics. He is set to start work as a mechanical engineer at General Electric in Lynn, Massachusetts in late August, 2011.

Permanent address: 100 Dogwood Lane
Wading River, NY 11792

This thesis was typeset with L^AT_EX[†] by the author.

[†]L^AT_EX is a document preparation system developed by Leslie Lamport as a special version of Donald Knuth's T_EX Program.